AD-A108 633 NAVAL RESEARCH LAB WASHINGTON DC F/G 20/3
STEADY STATE NUMERICAL SOLUTION OF MAGNETICALLY INSULATED CHARG--ETC(U)
DEC 81 R J BARKER, P F OTTINGER ES-77-A-81-6021
UNCLASSIFIED NRL-MR-4654 NL

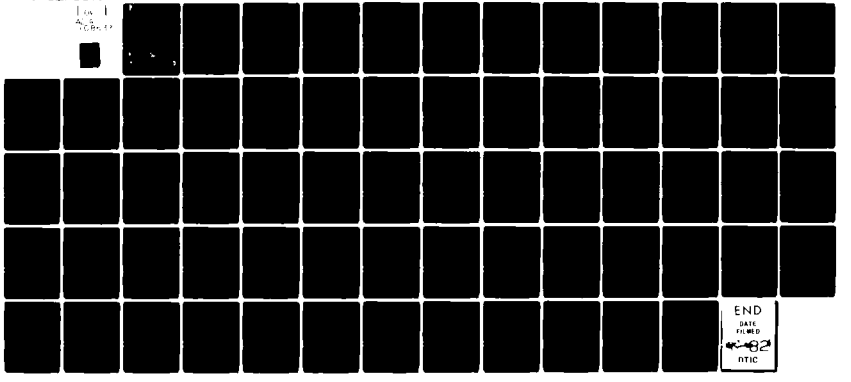

END
DATE FILMED
-82
DTIC

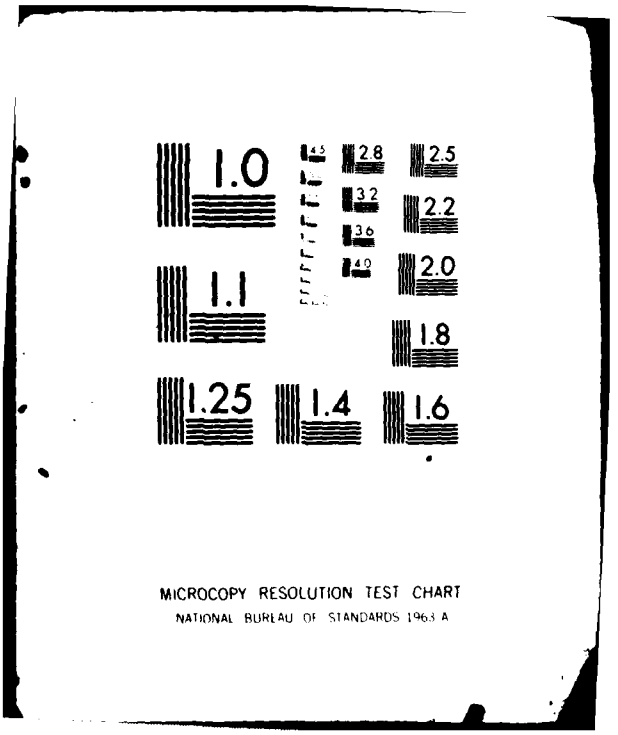
1.0
1.1
1.25
1.4
1.6
2.8
3.2
3.6
4.0
2.5
2.2
2.0
1.8
MICROCOPY RESOLUTION TEST CHART
NATIONAL BUREAU OF STANDARDS 1963 A

LEVEL II

NRL Memorandum Report 4584

AD A108633

Steady State Numerical Solution of Magnetically Insulated Charge Flow in Coaxial Geometry

R. J. Barker and P. F. Ottinger

JAYCOR, Inc.
Alexandria, VA 22304

December 8, 1981

This research was sponsored in part by the Defense Nuclear Agency under Subtask T99QAXLA014, work unit 46 and work unit title "Ion Beam Generation" and by the Department of Energy, Washington, D.C.

NAVAL RESEARCH LABORATORY
Washington, D.C.

SECURITY CLASSIFICATION OF THIS PAGE (When Data Entered)

REPORT DOCUMENTATION PAGE		READ INSTRUCTIONS BEFORE COMPLETING FORM
1. REPORT NUMBER NRL Memorandum Report 4654	2. GOVT ACCESSION NO. AD-A108633	3. RECIPIENT'S CATALOG NUMBER
4. TITLE (and Subtitle) STEADY STATE NUMERICAL SOLUTION OF MAGNETICALLY INSULATED CHARGE FLOW IN COAXIAL GEOMETRY		5. TYPE OF REPORT & PERIOD COVERED Interim report on a continuing NRL Problem 6. PERFORMING ORG. REPORT NUMBER
7. AUTHOR(s) R.J. Barker* and P.F. Ottinger*		8. CONTRACT OR GRANT NUMBER(s)
9. PERFORMING ORGANIZATION NAME AND ADDRESS Naval Research Laboratory Washington, DC 20375		10. PROGRAM ELEMENT, PROJECT, TASK AREA & WORK UNIT NUMBERS T99QAXLA014; NRL Problem 47-0875-0-1 (ES-77-A-01-6021; NRL Problem (47-0879-0-1)
11. CONTROLLING OFFICE NAME AND ADDRESS Department of Energy, Washington, DC 20545 Defense Nuclear Agency, Washington, DC 20305		12. REPORT DATE December 8, 1981 13. NUMBER OF PAGES 65
14. MONITORING AGENCY NAME & ADDRESS(if different from Controlling Office)		15. SECURITY CLASS (of this report) UNCLASSIFIED 15a. DECLASSIFICATION/DOWNGRADING SCHEDULE

16. DISTRIBUTION STATEMENT (of this Report)

Approved for public release, distribution unlimited.

17. DISTRIBUTION STATEMENT (of the abstract entered in Block 20, if different from Report)

18. SUPPLEMENTARY NOTES

*Present Address: JAYCOR, Inc., Alexandria, VA 22304

This research was sponsored in part by the Defense Nuclear Agency under Subtask T99QAXLA014, work unit 46 unit title "Ion Beam Generation" and by the Department of Energy, Washington, D.C.

19. KEY WORDS (Continue on reverse side if necessary and identify by block number)

20. ABSTRACT (Continue on reverse side if necessary and identify by block number)

A vectorized, FORTRAN computer program has been written to calculate steady-state electron and ion fluxes as well as radial profiles of the magnetic and electric fields for specific practical radial diode and magnetically insulated vacuum feed line parameters. The numerical formulation is derived in part from the theoretical treatment of the topic by K.D. Bergeron. However, it differs from the treatment in several important respects, including: a correction in

(Continued)

DD FORM 1 JAN 73 1473 EDITION OF 1 NOV 65 IS OBSOLETE
S/N 0102-014-6601

SECURITY CLASSIFICATION OF THIS PAGE (When Data Entered)

20. ABSTRACT (Continued)

one of the key scaling expressions, a restructuring of the boundary conditions to allow for specific parametric solutions, and a more careful consideration of the regions near the anode and cathode surfaces and near the electron sheath boundary. In deriving these results, analytic approximations for the fields in these "special" regions were developed. These approximate solutions permitted numerical treatment of the singularities there. Matching the approximations between the regions also provided first-order guesses for the gross steady-state operating characteristics.

CONTENTS

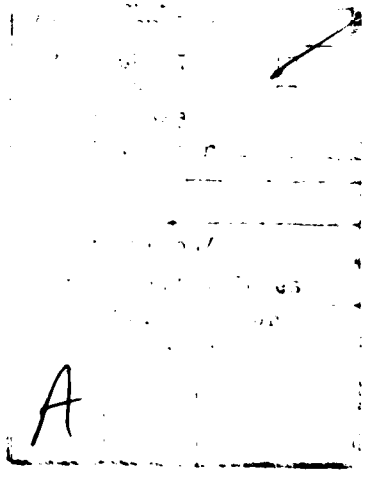

STEADY STATE NUMERICAL SOLUTION OF MAGNETICALLY INSULATED CHARGE FLOW IN COAXIAL GEOMETRY

I. INTRODUCTION

Impressive results have been achieved experimentally with the production of intense proton fluxes in radial diodes.[2-4] The high ion production efficiencies of these devices make them attractive candidates for use as driver sources in future ion beam inertial confinement fusion systems. In addition, magnetically insulated, coaxial vacuum feed lines[5-8] form an integral part of pulsed power systems for a wide variety of applications. Clearly, a computer code capable of predicting current flow in coaxial systems for realistic values of operational parameters would be a valuable tool. At the present time the only relativistic, two-specie, cylindrical geometry, theoretical formulation using cycloidal electron orbits is that of K. D. Bergeron.[1] Its foundation rests on the steady-state magnetic insulation model formulated independently by Sudan and Lovelace,[9,10] and at about the same time by Ron, Mondelli, and Rostoker.[11] In this model, electrons form a cloud near the cathode in which each electron traces an individual, single-arc trajectory which begins and terminates on the solid cathode surface (See Fig. 1.) All of these electrons see the full steady-state, self-consistent electric and magnetic fields during their entire orbit and all orbits are identical. There exists a competing magnetic insulation model formulated by Antonsen and Ott[12] and foreshadowed in the work of Creedon[13] and Buneman.[14] This model assumes that all electrons in the cathode sheath have been emitted from the cathode surface onto electrostatic equipotential contours during an adiabatically rising diode voltage pulse. In the equilibrium state, they $\vec{E} \times \vec{B}$ drift along their respective contours in a Brillouin[15] type flow, never again intersecting the cathode (See Fig. 1). This formulation is based on a vanishingly small Larmor radius approximation. The cylindrical geometry $\vec{E} \times \vec{B}$ drift model has recently been treated by Swegle and Ott.[16]

Manuscript submitted on September 9, 1981.

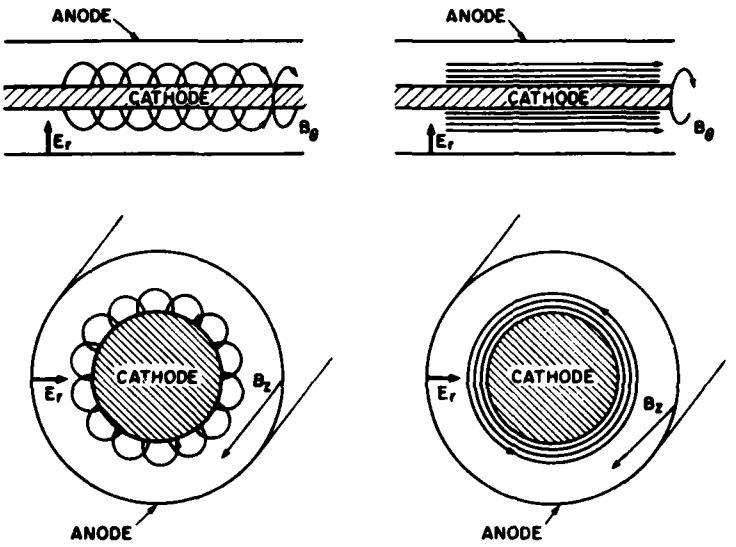

Fig. 1 — Two models for magnetically insulated electron flow: large orbit flow (left) and small larmor radius or Brillouin flow (right).

Both equilibrium models have equal physical validity. When applied to a given problem, they have led to very similar solutions,[17] however, stability properties could differ considerably. No sufficiently extensive analytic comparison has been performed on both models to justify the exclusion of one or the other for specific parameter ranges. However, there are conceptual weaknesses regarding the initiation of Brillouin flow in coaxial geometry. Certainly it can be postulated that appropriate injection mechanisms can be experimentally contrived, but this is not very satisfying when faced with the analysis of a general, uncontrived device. In addition, for the case of a radial diode with strong B_θ insulation, the $\vec{E} \times \vec{B}$ drift is axial. In time, this would deplete any initial Brillouin electron population. Injection and replenishment problems do not exist for the Sudan and Lovelace formulation. For that reason, it was chosen for use in this analysis. In reality, it seems probable that some mixture of the two distributions exists in magnetically insulated coaxial lines with the Antonsen and Ott picture dominating early in time and progressively giving way to Sudan and Lovelace electrons later in the pulse. A number of computer simulations have been conducted which seem to support such a picture.[18]

II. THE THEORETICAL MODEL

Cross-sections of both polarity types of the coaxial geometry treated in this analysis are depicted in Fig. 2. Unless otherwise stated, the central conductor is assumed to be the cathode in the following discussion. The analysis for the case of a central anode is identical except for magnetic field boundary conditions discussed at the end of this section. The major assumptions of the model are as follows:

(1) All emitted electrons are confined to an azimuthally symmetric electron sheath of radius, r_S, and execute identical single-arc trajectories out to that radius. The magnetic insulation field, $\vec{B}$, moderately exceeds the critical insulation field (defined as that field value at which electron orbits just graze the anode surface), so that $r_S < r_A$, where r_A is the anode radius and the critical fields are defined as

$$(B_z)_{\text{crit}} = \frac{m_0 c^2}{e} \left(\frac{2 r_A}{r_A^2 - r_c^2} \right) \sqrt{U_0^2 + 2U_0} ,$$

and

$$(B_\theta)_{\text{crit}} = \frac{m_0 c^2}{e} \frac{0.2\sqrt{U_0^2 + 2U_0}}{r_c \, 2 \ln\left(\frac{r_A}{r_c}\right)} .$$

Here r_c is the cathode radius and U_0 is the diode voltage multipled by $\frac{e}{m_0 c^2}$.

(2) The time-scale is such that the self-magnetic fields do not significantly penetrate the anode and cathode surfaces.

(3) The electrons are treated relativistically and the ions nonrelativistically (a reasonable approximation for voltages below 10 MV).

(4) The ion current is strictly radial. This implies no significant ion contribution to the self magnetic field. (The angular deflection suffered by an ion is on the order of $\sqrt{\frac{m_0}{M_0}} \frac{B}{B_{\text{crit}}}$ radians. Therefore, even if $B = 4B_{\text{crit}}$ an ion would experience less than 0.1 radian deflection.)

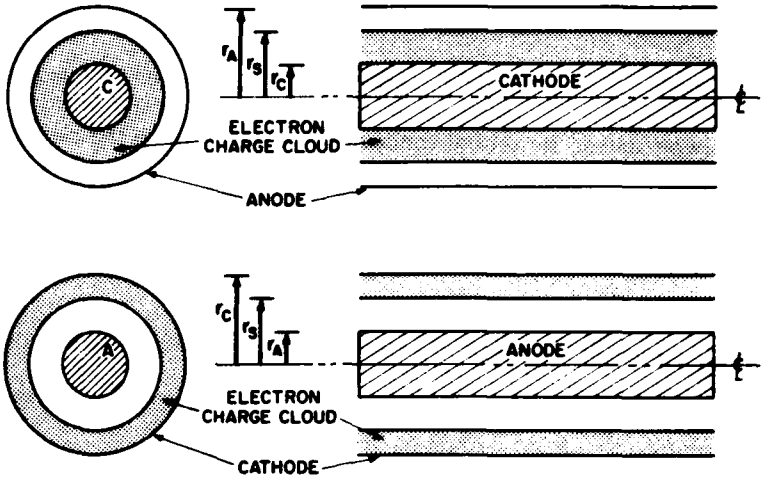

Fig. 2 — Coaxial, magnetic insulation geometries of the negative polarity (top) and positive polarity (bottom) types.

One characterizes the electron (ion) beam by a velocity $\vec{v}$ ($\vec{V}$), charge density $n(N)$, and current density $\vec{j} = n\vec{v}(\vec{J} = N\vec{V})$. Conservation of relativistic electron energy requires that

$$\gamma m_0 c^2 - e\phi(r) = m_0 c^2, \tag{1}$$

where $\gamma = \left[1 - \frac{v^2}{c^2}\right]^{-1/2}$. Conservation of canonical momentum demands that

$$\gamma m_0 v_{\parallel} - \frac{e}{c} A_{\parallel} = 0, \tag{2}$$

where the $\parallel$ subscript refers to the $\vec{E} \times \vec{B}$ direction. Finally, conservation of ion energy states that

$$V_r = \sqrt{\frac{2e}{M_0}}\sqrt{\phi_0 - \phi}, \tag{3}$$

where ϕ_0 is the imposed diode voltage. Continuity of diode current flux provides two additional constants, $F = r|J_r|$ and $f = -r|j_r|$. Employing all of these relations allows one to reduce Poisson's equation and Ampere's law to

$$\nabla^2\phi(r) = \frac{4\pi}{r}\left[2\left|\frac{f}{v_r}\right| - \left|\frac{F}{V_r}\right|\right], \tag{4}$$

and

$$(\vec{\nabla} \times (\vec{\nabla} \times \vec{A}(r)))_{\parallel} = -4\pi\left|\frac{2f}{cr v_r}\right| v_{\parallel}. \tag{5}$$

The factors of two for the electron flux terms reflect the presence of both radially inward and radially outward components to the electron current in the electron cloud. This doubling of the electron flow is specifically mentioned by Bergeron if Ref. 1; however, it is not present in his Eqs. (35) and (36).

Numerical considerations encourage the substitution of appropriately scaled dimensionless variables in place of those appearing in Eqs. (4) and (5). Following Bergeron, the terms employed in this analysis are $U \equiv \frac{e}{m_0c^2}\phi$, $W \equiv \frac{e}{m_0c^2}A_\theta$ [or $W \equiv -\frac{e}{m_0c^2}A_z$ for an *azimuthal* insulating field], and $\Lambda \equiv \frac{4\pi}{cB_0}\sqrt{\frac{M_0}{m_0}}|F|$. The electron flux term is modified by the additional factor of two mentioned above, giving $\lambda \equiv \frac{8\pi}{cB_0}|f|$. A significant modification to Bergeron's treatment can be found in the new scale chosen for the independent radial variable. It is here defined as $\rho \equiv \frac{eB_0}{m_0c^2}r$ where B_0 is chosen to be some typical magnetic field strength. In contrast, Bergeron scales r to the electron gyroradius in the presence of the magnetic field at the cathode surface. Such a scaling provides one with a simple boundary condition for the first derivation of W at ρ_c, namely $\left.\frac{dW}{d\rho}\right|_{\rho=\rho_c} = 1$. However, the value of $\vec{B}$ at $\rho = \rho_c$ is known *a priori* only for the case of an azimuthal insulation field with the cathode as the central conductor. In addition, the possibility of the magnetic field strength approaching and even equaling zero at the cathode surface for the other cases cannot be discarded. Such an eventuality would make nonsense of any solutions using Bergeron's scaling and may, at least in part, explain the lack of closed solutions Bergeron noted in some parameter regimes.

Given these definitions, Eqs. (4) and (5) reduce to

$$\rho\frac{d^2U}{d\rho^2} + \frac{dU}{d\rho} = \frac{\lambda(1+U)}{\sqrt{U^2+2U-W^2}} - \frac{\Lambda}{\sqrt{U_0-U}}, \tag{6}$$

and

$$\rho\frac{d^2W}{d\rho^2} + \frac{dW}{d\rho} = \frac{\lambda W}{\sqrt{U^2+2U-W^2}} + \epsilon\frac{W}{\rho}, \tag{7}$$

with $\epsilon = 0$ for azimuthal insulation and $\epsilon = 1$ for the axial case. The boundary conditions for axial insulation are

$$U(\rho_c) = W(\rho_c) = \left.\frac{dU}{d\rho}\right|_{\rho_c} = 0, \tag{8}$$

at the cathode while at the anode

$$U(\rho_A) = U_0 \text{ and } \left.\frac{dU}{d\rho}\right|_{\rho_A} = 0. \tag{9}$$

The conditions governing the first derivative of U follow directly from the assumption of space charge limited, Gaussian emission at both surfaces. (However, if an equilibrium solution is sought for which $\Lambda = 0$, then the value of the electric field at the anode cannot be assumed to vanish.) Such an emission mechanism in turn presumes a sufficiently dense plasma to exist at both surfaces. We now have a set of two second order equations in U and W, with two additional unknowns, λ and Λ. Six boundary conditions are therefore necessary for a solution. In addition to the five conditions stated in Eqs. (8) and (9), for the case of axial magnetic insulation, the final condition results from conservation of the magnetic flux,

$$\Phi_M = \int_S \vec{B} \cdot d\vec{a} = \oint_C \vec{A} \cdot d\vec{S},$$

over a fixed cross sectional surface area, S, enclosed by the line contour, C. Specifically, it is assumed that the insulating B-field is present before emission begins and that any diffusion of the field into the electrodes is insignificant over the time scale of the voltage pulse. For the case of an initially uniform, axial insulating field, B_0, which is taken as the scaling field for ρ, this condition implies

$$W(\rho_A) = \frac{\rho_A^2 - \rho_c^2}{2\rho_A}. \tag{10}$$

On the other hand, for an azimuthal insulating field, magnetic flux is not conserved. In place of Eq. (10) one is given the known magnetic field strength at the surface of the central conductor,

$$B_{c.c.} = 0.2\,\frac{I_{c.c.}}{R_{c.c.}}, \tag{11}$$

where $B_{c.c.}$ is in gauss, $R_{c.c.}$ is the radius of the central conductor measured in centimeters and $I_{c.c.}$ is the current in amperes flowing through the central conductor. Therefore, the final boundary condition for the azimuthal field case is simply

$$\left.\frac{dW}{d\rho}\right|_{\rho_{c.c.}} = \frac{B_{c.c.}}{B_0}, \tag{12}$$

where B_0 is the arbitrary scale field and $\rho_{c.c.}$ may be either ρ_A or ρ_c, depending upon the geometry chosen. (When $B_0 = B_{c.c.}$ and $\rho_{c.c.} = \rho_c$, this reduces to Bergeron's boundary condition.) For the case of a magnetically self-insulated vacuum feed line, the value of $I_{c.c.}$ is a known (or at least independently derivable) quantity. On the other hand, $I_{c.c.}$ is not known *a priori* for a radial diode. In this device, the central conductor current will generally be a function of the axial dimension, z. Furthermore, the total current, $I_{c.c.}$, flowing through the diode will be entirely due to ion flow through the A-K gap and will be given in statamps by

$$I_{c.c.} = 2\pi |rJ_r| L,$$

or

$$I_{c.c.} = 2\pi L\left[\frac{cB_0}{4\pi}\sqrt{\frac{2m_0}{M_0}}\,\Lambda\right], \tag{13}$$

where L is the axial half-length of the gap. In order to clarify the distinctions between the axial versus the azimuthal boundary conditions and unknowns, they are grouped accordingly in Table 1.

For both cases, the numerical integration of Eqs. (6) and (7) begins at the cathode radius, ρ_c. For a configuration with B_z insulation, values are guessed for λ, Λ, and $W'(\rho_c)$. Then U, U', and W are integrated out to the anode radius and their boundary values are compared to those given in (9) and (10). Repeated guesses for λ, Λ, and $W'(\rho_c)$ are made until a match-up at ρ_A is achieved. For B_θ insulation with the cathode as the central conductor, an additional starting condition is given in the form of Eq. (12). This simplifies the problem considerably. Only the two anode conditions given by Eq. (9) must be matched and only values for λ and Λ must be sought by iterative guesses. Finally, for the azimuthal case with the anode as the central conductor, the guessed parameters become $\lambda, W'(\rho_c)$, and $I_{c.c.}$. The three conditions which must be matched at ρ_A are now given by Eqs. (9) and (12). It

Table 1. Matrix of Knowns, Unknowns, and Boundary Conditions.

Insulating B-field Type	AXIAL		AZIMUTHAL			
Relative A-K Positions	either		cathode inside		cathode outside	
Ions Present ?	Yes	No	Yes	No	Yes	No
Input Parameters	$(B_z)_o$	$(B_z)_o$	L	$I_{c.c.}$	L	$I_{c.c.}$
Input $\rho = \rho_c$ Guesses	j, J, and W'	j, W'	j, J	j	j, J and W'	j, W'
Output Quantities to be matched at $\rho = \rho_A$ and at $\rho = \rho_S$	U, U', and W	U, W	U, U'	U	U, U', and W'	U, W'
Universal Input	r_A, r_C, φ_o, LAZ, LCIN, and LIONS					
Universal Output	Radial Profiles of φ and B					

where: r_A (r_C) = anode (cathode) radius in centimeters,
φ_o = A-K potential difference in volts,
$(B_z)o$ = imposed insulating axial magnetic field strength in gauss,
L = axial length of A-K gap in centimeters,
$I_{c.c.}$ = current flowing in the central conductor in amperes, and
j (J) = electron (ion) current density at cathode in amp/cm^2.

will be shown in the next section that analytic solutions are available for the region between ρ_A and ρ_S. This allows for numerical solution matching at ρ_S instead of at ρ_A with a considerable gain in accuracy.

A problem arises when solutions are sought for radial diodes in which both axial *and* azimuthal magnetic insulating fields are present. If no B_z is imposed in the A-K gap, then only pure azimuthal insulation is possible and no conflict can arise. When an axial insulation case with ion flow is being studied, however, it is inevitable that a B_θ be generated as well. The strength of this B_θ in the A-K gap can be predicted directly from the value of Λ obtained in the pure B_z solution. If this field strength is comparable to or greater than the imposed B_z, the numerical formulation presented here has more limited value for predicting actual diode operating characteristics. (See Appendix B.)

III. THE COMPUTATIONAL FORMULATION

As previously stated, the solution of Eqs. (6) and (7), combined with the boundary conditions in Eqs. (8) and (9), will be carried out as a three-parameter "shooting" problem. Values must be guessed for λ, Λ, and $\left.\frac{dW}{d\rho}\right|_{\rho_c}$ and the equations then integrated from ρ_c to ρ_A. The correctness of a given guess is determined by the accuracy with which generated function values match with known solutions at ρ_A and ρ_S. In undertaking the numerical integration of Eqs. (6) and (7), special attention must be paid to three separate values of ρ at which certain terms on the right hand side become singular. Specifically, the denominator of the electron current term vanishes at $\rho = \rho_c$, since both U and W are defined to be equal to zero there. It also vanishes at the electron sheath boundary, $\rho = \rho_S$, as would be expected, since this quantity represents the radial component of the electron velocity. The final singularity occurs at $\rho = \rho_A$ where the ion current term in Eq. (6) becomes infinite. Brute force numerical procedures cannot cope with integrations in the neighborhood of these singular points. Instead, analytic treatments expanding about the singularities produce approximate explicit solutions valid in the pathological regions near ρ_c and ρ_S. This technique provides the numerical quadrature with tractable starting values at $\rho = \rho_c + \Delta\rho$. The numerics may be relied upon from that point up to about $\rho = \rho_S - \Delta\rho$ at which radius another analytic approximation advances the solution to ρ_S. Beyond that point, λ equals zero. Equations (6) and (7) have straightforward analytic solutions spanning $\rho_S < \rho \leqslant \rho_A$ which can be used to accurately advance U, W $\left[\text{or } \frac{dW}{d\rho}\right]$, and $\frac{dU}{d\rho}$ at $\rho = \rho_S$ out to the anode radius. In this manner, the numerical singularity at $\rho = \rho_A$ need never be faced directly.

The numerical solution of Eqs. (6) and (7) begins with the derivation of an explicit functional expression for the radial variations of U and W in the immediate vicinity of the cathode surface. For $\rho = \rho_c + r$ where $r << \rho_c$, the equations can be expanded and solved in terms of a triple power series with solutions

$$U = \left(\frac{r}{\rho_c}\right) \sum_{n=0}^{\infty} a_n^{(1)} \left(\frac{r}{\rho_c}\right)^n + \left(\frac{r}{\rho_c}\right)^{4/3} \sum_{n=0}^{\infty} a_n^{(4/3)} \left(\frac{r}{\rho_c}\right)^n + \left(\frac{r}{\rho_c}\right)^{5/3} \sum_{n=0}^{\infty} a_n^{(5/3)} \left(\frac{r}{\rho_c}\right)^n. \tag{14}$$

$$W = \left[\frac{r}{\rho_c}\right] \sum_{n=0}^{\infty} b_n^{(1)} \left[\frac{r}{\rho_c}\right]^n + \left[\frac{r}{\rho_c}\right]^{4/3} \sum_{n=0}^{\infty} b_n^{(4/3)} \left[\frac{r}{\rho_c}\right]^n + \left[\frac{r}{\rho_c}\right]^{5/3} \sum_{n=0}^{\infty} b_n^{(5/3)} \left[\frac{r}{\rho_c}\right]^n. \tag{15}$$

Straightforward calculus and algebra may then be used to isolate the leading order terms,

$$U = \frac{3}{2}\left[\frac{3\lambda^2\rho_c^2}{4}\right]^{1/3}\left[\frac{r}{\rho_c}\right]^{4/3} + \left[\frac{b_c^2\rho_c^2}{20} - \frac{9\Lambda\rho_c}{20U_0^{1/2}}\right]\left[\frac{r}{\rho_c}\right]^2, \tag{16}$$

and

$$W = (-1)^{\epsilon+1} b_c r\left[1 - \frac{1}{2}\left[\frac{r}{\rho_c}\right] + \frac{9}{28}\left[\frac{2\lambda^2\rho_c^2}{9}\right]^{1/3}\left[\frac{r}{\rho_c}\right]^{4/3}\right], \tag{17}$$

where the term $b_c \equiv \dfrac{B(\rho_c)}{B_0}$ is presently unknown and where the solutions are only valid for

$$\frac{r}{\rho_c} < Min\left[\frac{40}{9}\left[\frac{10}{3}\right]^{1/2}\frac{\lambda V_0^{3/4}}{\Lambda^{3/2}\rho_c^{1/2}},\ \frac{9\lambda}{2b_c^3\rho_c^2}\right]. \tag{18}$$

Equation (18) places an upper limit on the initial step size. All but the ion term in Eq. (16) had been predicted by the leading order terms of an expression due to Goldstein[19] which corrected the Child-Langmuir emission law to include transverse magnetic field effects. The first derivatives of equations (16) and (17) are simply

$$U' = \frac{dU}{d\rho} = \frac{dU}{dr} = 2\left[\frac{3}{4}\frac{r}{\rho_c^2}\right]^{1/3}\lambda^{2/3} + \frac{r}{10}\left[b_c^2 - \frac{9\Lambda}{\rho_c U_0^{1/2}}\right], \tag{19}$$

and

$$W' \equiv \frac{dW}{d\rho} = \frac{dW}{dr} = (-1)^{\epsilon+1} b_c\left[1 - \frac{r}{\rho_c} + \frac{3}{4}\left[\frac{2}{9}\lambda^2\rho_c^2\right]^{1/3}\left[\frac{r}{\rho_c}\right]^{4/3}\right]. \tag{20}$$

For purposes of the overall numerical quadrature of Eqs. (6) and (7), the gap region between ρ_c and ρ_A is divided up into some predetermined number of identical, one-dimensional cells of width, $\Delta\rho$. The above approximations are used to advance the solution of U, W, U', and W' over the first $\Delta\rho$ away from the $\rho = \rho_c$ singularity point.

The bulk of the remaining numerics is accomplished using a proven predictor-corrector scheme. Unfortunately, this scheme requires a knowledge of functional values at four prior spatial steps in order to advance an additional $\Delta\rho$. In order to obtain those additional values at the start of the integration, a

fourth-order Runga Kutta scheme is employed.[20] For this, as well as for the predictor-corrector, the set of two second-order D.E.'s is reduced to a set of four first-order D.E.'s as follows:

$$U' \equiv X, \tag{21}$$

$$X' = \frac{\lambda(1+U)}{\rho\sqrt{S}} - \frac{\lambda}{\rho\sqrt{U_0 - U}} - \frac{X}{\rho}, \tag{22}$$

$$W' \equiv Y, \text{ and} \tag{23}$$

$$Y' = \frac{\lambda W}{\rho\sqrt{S}} + \frac{W}{\rho^2} - \frac{Y}{\rho}, \tag{24}$$

where $S \equiv U^2 + 2U - W^2$. Each expression is then in the form $\eta' = f_\eta(\rho, U, W, X, Y)$ and can be advanced one $\Delta\rho$ at a time using the standard R-K approximation,

$$\eta_{n+1} = \eta_n + \frac{1}{6}(k_{\eta 1} + 2k_{\eta 2} + 2k_{\eta 3} + k_{\eta 4}),$$

where

$$k_{\eta 1} = \Delta\rho f_\eta(\rho_n, U_n, W_n, X_n, Y_n),$$

$$k_{\eta 2} = \Delta\rho f_\eta(\rho_n + \frac{1}{2}\Delta\rho, U_n + \frac{1}{2}k_{U1}, W_n + \frac{1}{2}k_{W1}, \ldots),$$

$$k_{\eta 3} = \Delta\rho f_\eta(\rho_n + \frac{1}{2}\Delta\rho, U_n + \frac{1}{2}k_{U2}, W_n + \frac{1}{2}k_{W2}, \ldots),$$

$$k_{\eta 4} = \Delta\rho f_\eta(\rho_n + \Delta\rho, U_n + k_{U3}, W_n + k_{W3}, \ldots).$$

Thereafter, the Adams-Bashforth-Moulton predictor-corrector scheme[21] advances the variables in a two-step process:

$$(\eta_{n+1})_{\text{predicted}} = \eta_n + \frac{\Delta\rho}{24}(55\eta'_n - 59\eta'_{n-1} + 37\eta'_{n-2} - 9\eta'_{n-3}).$$

and

$$(\eta_{n+1})_{\text{corrected}} = \eta_n + \frac{\Delta\rho}{24}(9\eta'_{n+1} + 19\eta'_n - 5\eta'_{n-1} + \eta'_{n-2})$$

where η'_{n+1} has been calculated using the predicted value for η_{n+1}. An error check is accomplished by monitoring the magnitude of $|(\eta_p - \eta_c)/\eta_p|$ where η_p and η_c are the predicted and corrected values of η, respectively.

The above predictor-corrector process is continued until the electron sheath radius, ρ_S, is reached. At that point, another analytic approximation must be found in order to correctly advance the function values past the numerical singularity there. This is accomplished by expanding Eqs. (6) and (7) about ρ_S in a power series. One may write $\rho = \rho_S - r$, $U = U_S + \hat{U}$, and $W = W_S + \hat{W}$ where

$$\rho_S >> r > 0,$$

$$\hat{U} = a_0 r^{\alpha_0} + a_1 r^{\alpha_1} + a_2 r^{\alpha_2} + \ldots,$$

$$\hat{W} = b_0 r^{\beta_0} + b_1 r^{\beta_1} + b_2 r^{\beta_2} + \ldots,$$

and

$$U_S^2 + 2U_S - W_S^2 = 0.$$

Equations (6) and (7) can then be expanded and solved. The leading terms of the solutions are

$$U = U_S + a_0 r + a_1 r^{3/2} + a_2 r^2, \tag{25}$$

and

$$W = W_S + b_0 r + b_1 r^{3/2} + b_2 r^2, \tag{26}$$

where

$$2(1 + U_S)a_0 - 2W_S b_0 > 0,$$

$$a_1 = \frac{4\lambda(1 + U_S)}{3\rho_S[2(1 + U_S)a_0 - 2W_S b_0]^{1/2}},$$

$$b_1 = \frac{4\lambda W_S}{3\rho_S[2(1 + U_S)a_0 - 2W_S b_0]^{1/2}},$$

$$a_2 = \frac{(a_0 - \Lambda/(U_0 - U_S)^{1/2})}{2\rho_S},$$

and

$$b_2 = \frac{(b_0 - \epsilon W_S/\rho_S)}{2\rho_S}.$$

As is obvious from Eqs. (25) and (26), the coefficients a_0 and b_0 are merely the negative first derivatives of U and W, respectively at ρ_S (i.e., $a_0 = -U_S' = -X_S$ and $b_0 = -W_S' = -Y_S$). Having used Eqs. (25) and (26) to obtain U_S, W_S, X_S and Y_S, the numerical integration of Eqs. (6) and (7), with λ now set equal to zero, may resume. In the RADBER code, however, explicit analytic expressions are used to match all functions of interest at ρ_S from the known values at the anode radius.

Beyond the electron sheath radius, the key deterministic equations for the electrostatic and magnetostatic potentials become

$$\rho \frac{d^2U}{d\rho^2} + \frac{dU}{d\rho} = \frac{\Lambda}{\sqrt{U_0 - U}}, \tag{27}$$

and

$$\rho \frac{d^2W}{d\rho^2} + \frac{dW}{d\rho} = \epsilon \frac{W}{\rho}. \tag{28}$$

Equation (27) takes the same form as the equation treated by Langmuir in his 1913 paper[22] and later treated in greater depth for coaxial geometry in a subsequent paper by Langmuir and Blodgett.[23] The solution to the equation is therefore

$$U = U_0 - \left\{\frac{9}{4}\,\rho\beta^2\Lambda\right\}^{2/3} \tag{29}$$

where $\beta = \Sigma A_n \gamma^n$ and $\gamma \equiv \ln\left[\frac{\rho}{\rho_A}\right]$. The first 14 values of the coefficients, A_n, are listed in Blodgett's paper. Knowing the values of U_0, Λ, ρ_A, and ρ_S, a value for U_S may be calculated using Eq. (29). This value is then compared to that found via the numerical integration of Eq. (6) out from ρ_c. The closeness of the match is used to measure the accuracy of the original set of parameter guesses. For the case where $\Lambda = 0$ (i.e., no ion flow) Eq. (27) becomes

$$\rho\,\frac{d^2U}{d\rho^2} + \frac{dU}{d\rho} = 0, \tag{30}$$

with solution

$$U = U_S + X_S\rho_S \ln\left[\frac{\rho}{\rho_S}\right], \tag{31}$$

and the same matching procedure for U_S may be carried out. Similarly, the solutions to Eq. (28) take the form

$$W = \begin{cases} \left(W_S - \dfrac{a_{01}}{\rho_S}\right)\dfrac{\rho}{\rho_S} + \dfrac{a_0}{\rho}, & \epsilon = 1 \\ W_S + a_{02}\ln\left[\dfrac{\rho}{\rho_S}\right], & \epsilon = 0 \end{cases} \tag{32}$$

Matching the solutions for the first derivatives at $\rho = \rho_S$ demands that $a_{01} = \frac{1}{2}\,(W_S\rho_S - Y_S\rho_S^2)$ for the $\epsilon = 1$ case and $a_{02} = Y_S\rho_S$ for the $\epsilon = 0$ case. Equations (29), (31), and (32) may be used to obtain values for U_S, X_S, W_S, and Y_S in terms of known quantities. Depending upon the specific configuration under study, some subset of those four values (see Table 1) are matched to the corresponding values on the cathode side of the electron sheath boundary as obtained from Eqs. (25) and (26). The closeness of that fit at $\rho = \rho_S$ of the two sets of solutions forms the final, most accurate test of the validity of the original parameter guesses.

IV. APPROXIMATE ANALYTIC SOLUTION

For the case of low voltages and with geometries whose anode-cathode gap is much smaller than the radius of the outer conductor, complete, approximate analytic solutions can be obtained by matching the analytic solutions near the cathode given in Eqs. (16)-(20) with the solutions valid near the electron sheath radius given in Eqs. (25) and (26). The solutions are matched at $\rho_1 = (\rho_c + \rho_S)/2$ by requiring that U, W, U', and $B/B_0 = (W' + \epsilon W/\rho)$ all be continuous at $\rho = \rho_1$. At $\rho = \rho_S$ the solution given in Eqs. (25) and (26) is also matched in the same manner with the solution valid for $\rho_S \leqslant \rho \leqslant \rho_A$. There one finds

$$U = U_0 - \left[\frac{9}{4}\,\Lambda\rho_A\right]^{2/3}\left[\frac{r}{\rho_A}\right]^{4/3}, \tag{33}$$

and

$$W = \begin{cases} \dfrac{b_A}{2}\left[\rho - \dfrac{\rho_S^2}{\rho}\right] + \dfrac{\rho_S W_S}{\rho}, & \text{for } \epsilon = 1 \\ W_S + \rho_A b_A \ln\left[\dfrac{\rho}{\rho_S}\right], & \text{for } \epsilon = 0 \end{cases}, \tag{34}$$

where $r \equiv \rho_A - \rho$ and $b_A \equiv B(\rho_A)/B_0$. Equation (33) is equivalent to the limit of Eq. (29) for $r \ll \rho_A$. Likewise, Eq. (34) follows from Eq. (32) when a_0 is obtained by imposing the boundary conditions at $\rho = \rho_A$ instead of at $\rho = \rho_S$. For $\epsilon = 1$, flux conservation fixes the value of $W(\rho = \rho_A)$ (see Eq. (10)) and yields $b_A = [(\rho_A^2 - \rho_c^2)/(\rho_A^2 - \rho_S^2) - 2\rho_S W_S/(\rho_A^2 - \rho_S^2)]$. For the azimuthal field case ($\epsilon = 0$), on the other hand, $b_A = Y_A$ in agreement with Eq. (32) since the field outside the sheath is constant. In order to complete the overall solution for this analytic approximation one must also use the relationship, $U_S^2 + 2U_S - W_S^2 = 0$, and also $b_c = 1$ for the $\epsilon = 0$ case. There is now enough information with which to construct a composite solution.

For the case where the central conductor is the cathode, one finds that for both $\epsilon = 0$ or 1, an analytic solution is possible as long as the diamagnetic electron current does not significantly alter the magnetic field. In this case B_0 is approximately given by the applied field,

$$\frac{J(\rho_A)}{J_{CL}} = \left[\frac{6}{7}\right]^{3/2} \frac{d^2(U_S/U_0)^{3/2}}{[d - (U_S^2 + 2U_S)^{1/2}](U_S^2 + 2U_S)^{3/4}}, \tag{36}$$

$$\frac{j(\rho_c)}{j_{CL}} = \frac{6}{7}\left[\frac{3}{7}\right]^{1/2} \frac{d^2(U_S/U_0)^{3/2}}{(U_S^2 + 2U_S)}, \tag{37}$$

and

$$\rho_S - \rho_c = (U_S^2 + 2U_S)^{1/2}, \tag{38}$$

where $d = \rho_A - \rho_c$ and $j_{CL} = \left[\frac{m_i}{m_e}\right]^{1/2} J_{CL} = (2e/m_e)^{1/2}\ \phi_0^{3/2}/9\pi(r_A - r_c)^2$. The sheath potential needed to complete Eqs. (36)-(38) is defined by the transcendental equation

$$U_0 = \frac{U_S}{7}\left[1 + \frac{6d}{(U_S^2 + 2U_S)^{1/2}}\right]. \tag{39}$$

The ion production efficiency of the diode, $\eta = J/(J + j)$, can be easily obtained from Eqs. (36) and (37). Plots of J and $\rho_S - \rho_c$ are shown in Figs. (3) and (4) as solid lines. The validity of the results becomes suspect beyond $e\phi_0/m_e c^2 \sim 1$. Note that $|\rho_A - \rho_c| = d << \rho_A$ was also assumed which implies these results only apply to large radius structures with small anode-cathode gaps (i.e., large aspect ratio devices). For higher voltages and smaller aspect ratio devices the RADBER code is needed since in these cases the simple matching technique used to form the composite analytic solution is no longer possible. This results from the decreasing range of validity of the expansions used to obtain the solution. In any case, however, these approximate solutions may be used to provide reasonable starting parameter guesses for the RADBER code.

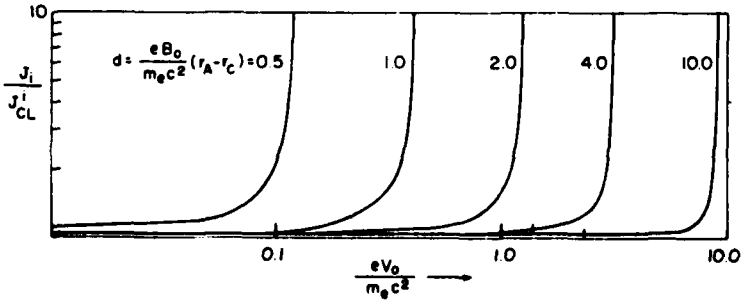

Fig. 3 — Analytic estimates for ion current enhancement

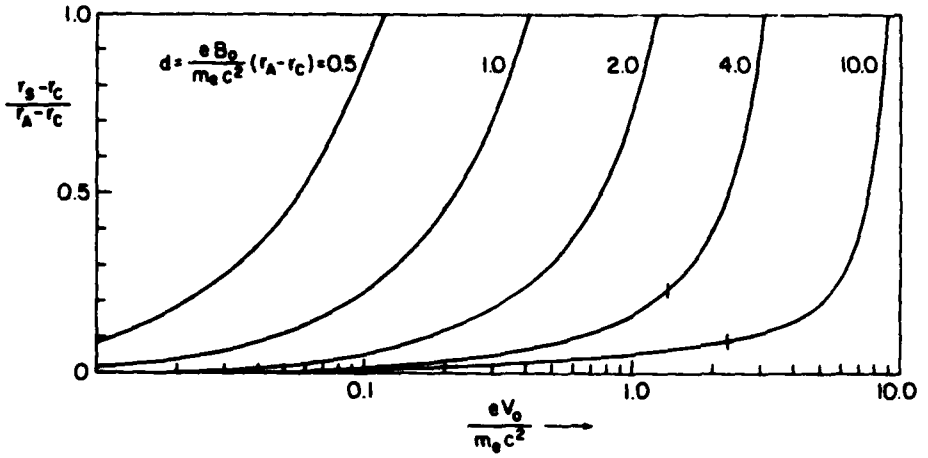

Fig. 4 — Analytic estimates for electron sheath thickness

V. THE NUMERICAL TREATMENT

The RADBER computational package consists of a main core program and four subprograms: START, PRIME, BOUND, and MATCH. All of these program elements are listed in their entirety in Appendix A. They are written in a version of FORTRAN compatible with the Texas Instruments Advanced Scientific Computer.[24] Every effort was made to avoid non-standard terminology. Nevertheless, the need for minor changes can be anticipated when implementing this code at any other computer facility. Particularly prone to such changes are the data input/output statements. For that reason, I/O formats were left as simple as possible. A particularly strong point of the code is its vectorized format. This allows for the simultaneous, step-by-step integration of U and W for a large number of λ and Λ guesses in a "shotgun" fashion. The average cost for the complete integration of Eqs. (6) and (7) over 500 steps from ρ_c to ρ_A for a single (λ, Λ, $W'(\rho_c)$) guess was about \$0.025. (CPU rates are over \$900/hour on the ASC at NRL.)

The basic flow chart for RADBER is shown in Fig. 5. In the main program, data input begins with a choice for the parameter, NDR, the number of radial steps across the anode-cathode gap. The default value, as shown, is 500. The specific physical and numerical parameters for the problem under study are fed in through the NAMELIST's, GUESS and GIVEN. For the sake of practicality, the code

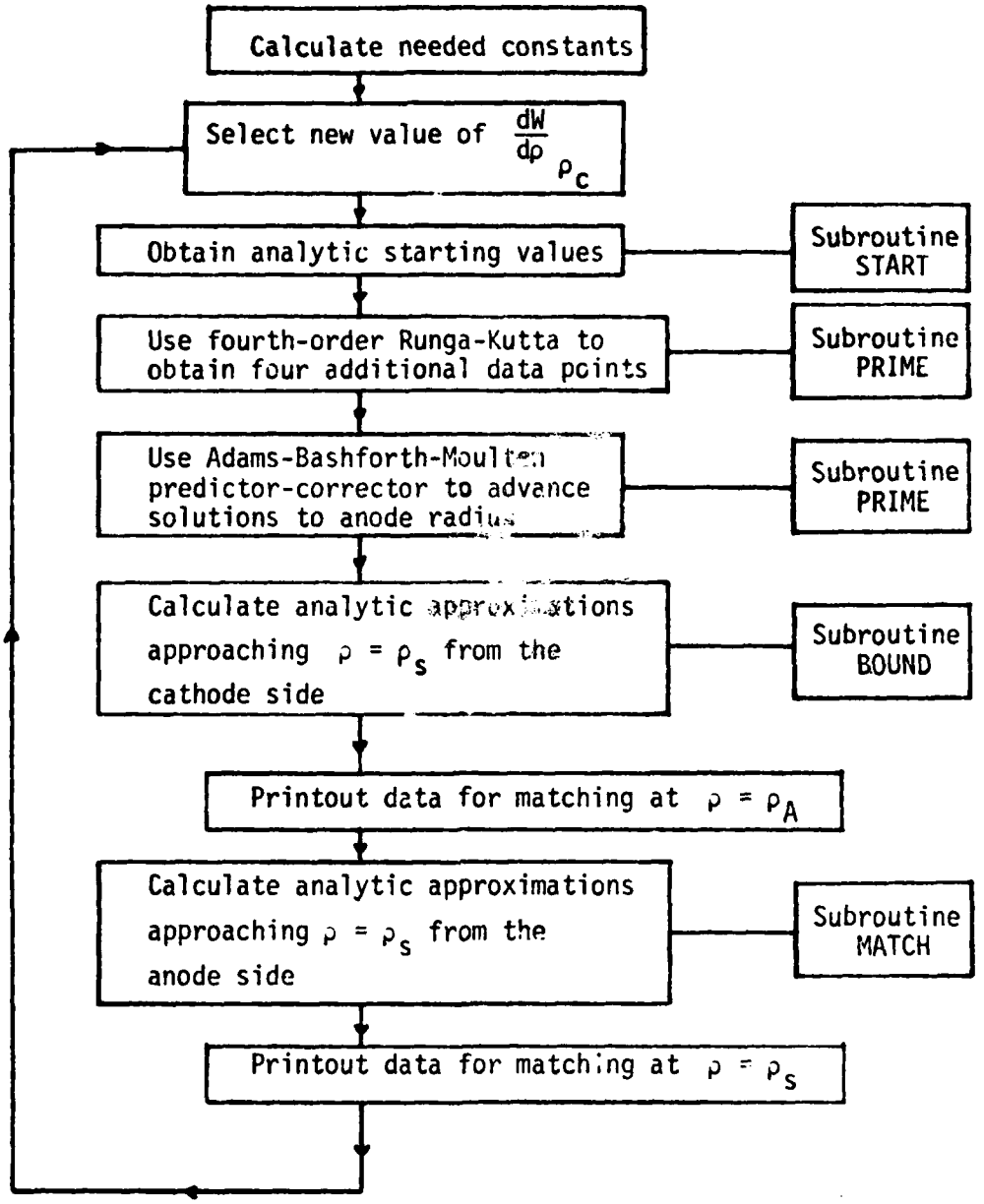

Fig. 5 — RADBER flow chart

accepts guesses for the actual current densities, j and J, at the cathode rather than for the dimensionless fluxes, λ and Λ. In GUESS, the range of guesses for the triplets, $(j, J, W'(\rho_c))$ are specified. The minimum guess for the electron current density is AMIN in amperes per cm.^{2} A total of NA values of j are then tried in the program, each one DELA greater than the next. Similarly, there are NB guesses for J in amps/cm^2 beginning with BMIN and increasing in steps of DELB. The product NA multiplied

by NB must equal exactly 100 for the program as presently written. Finally, the slopes of W at the cathode radius are guessed as some fraction, FMIN, FMIN + DELF, FMIN + 2 DELF, etc., of the scale magnetic field, B_0. There is no limit on the number, NF, of these which can be tested with the 100 (j,J) guesses under consideration. The significance of the integers, I1, I2, and I3 will be explained when the OUTPUT section of the program is discussed.

In NAMELIST, GIVEN, the cathode and anode radii are specified in centimeters by RC and RANODE, respectively. The potential difference between the two electrodes is given in volts by U_0. The scale magnetic field strength, B_0, in gauss, is arbitrary, but can conveniently be chosen as the vacuum, imposed field strength for an axial insulation field problem or as the vacuum value near the cathode for an azimuthal insulating field. The parameter, GAPLEN, is only significant when azimuthal insulation in a radial diode configuration (i.e., the cathode is the central conductor) is under study. In that case, it is equal to the axial length of the A-K gap in centimeters. In a similar sense, CURCEN need only be specified for the case of azimuthal insulation with no ion flow present. It is equal to the axial current assumed to be present in the central conductor in amperes. The logical variables, LAZ, LCIN, and LIONS specify the overall nature of the problem under consideration as follows:

a. LAZ = .TRUE. implies an azimuthal magnetic insulation field,

b. LCIN = .TRUE. implies the cathode is the central conductor, and

c. LIONS = .TRUE. implies the presence of ion (proton) flow.

Finally, ERROR is a decimal fraction to be chosen as the maximum allowable percentage difference tolerable in predictor-corrector steps before a given step iteration there is stopped.

RADBER then uses the above NAMELIST inputs in order to calculate constants and parameters utilized throughout the rest of the program. These set of one hundred guesses for (j,J) are then attempted for each guess of $\frac{dW}{d\rho}(\rho = \rho_c)$. That is, the entire remainder of the program is cycled through once for each value of $W'(\rho_c)$. This iteration begins at statement number 400. The 100

integrations from ρ_c to ρ_A for each (j,J) pair are carried out simultaneously. Quadrature over the first $\Delta\rho$ is accomplished in the subroutine, START, using the analytic approximations of Eqs. (16)-(20). From that point and over the next 4 $\Delta\rho$, fourth-order Runga-Kutta is employed to generate a finite length string of starting values for the master predictor-corrector scheme. Both here, as well as in the main integrator, the values for the second derivatives of $U(\rho)$ and $W(\rho)$ are calculated via Eqs. (6) and (7) in the subroutine, PRIME. That subroutine also locates the electron sheath radius, ρ_s, by monitoring the value of $U^2 + 2U - W^2$ and finds the effective anode radius for a given (j,J) by pinpointing the value of ρ for which $U(\rho) = U_0$. The Adams-Bashforth-Moulton predictor-corrector algorithm integrates "over" $\rho = \rho_S$, ignoring any functional discontinuities there. It simply forges ahead in a brute force manner, setting λ equal to zero between ρ_S and ρ_A. For some choices of parameter ranges, this may lead to serious errors propagating in the quadrature beyond $\rho = \rho_S$. For that reason, the array, IFLAG, stores the integer number of the radial step over which the electron sheath boundary was encountered. The final test for the validity of the various $(j,J,W'(\rho_c))$ guesses is accomplished through matching of the potentials and the fields at $\rho = \rho_S$.

After the predictor-corrector has blindly pushed all 100 integrations out to $\rho = \rho_A$, the program looks back to find the function values at the two data points immediately preceeding each of the 100 respective ρ_S's. Having stored those values in the COMMON block, FIT, the program then calls the subroutine, BOUND, to calculate U, $U'(=X)$, W, and $W'(=Y)$ at ρ_S (approaching from the cathode side) via the analytic approximations given in Eqs. (25) and (26). Specifically, the lowest order terms of those equations may be rearranged to yield

$$U_S = U_{n-1} + X_S r + a_1 r^{3/2}, \tag{40}$$

$$W_S = W_{n-1} + Y_S r + b_1 r^{3/2}, \tag{41}$$

where the subscript $(n-1)$, signifies the function value at the second data point before the recorded ρ_S. Equation (40) is multiplied by W_S and (41) by $(1 + U_S)$. Subtraction of the resultant equations leads to the expression

$$r = \frac{W_{n-1}(1 + U_S) - W_S(1 + U_{n-1})}{X_S W_S - Y_S(1 + U_S)}. \tag{42}$$

but, since $U_S^2 + 2U_S - W_S^2 = 0$,

$$r = \frac{(U_S^2 + 2U_S)^{1/2}(1 + U_{n-1}) - W_{n-1}(1 + U_S)}{Y_S(1 + U_S) - X_S(U_S^2 + 2U_S)^{1/2}}. \tag{43}$$

Using the known values of U_n as reasonable first guesses for U_S, Eq. (43) yields a first predicted value for r. That value can then be fed into (25) to obtain a corrected value for U_S and the process continued until reasonable convergence is achieved. As written, the subroutine BOUND performs a number of iterations equal to the integer, ITER, which is a fixed parameter in the CALL statement.

At that point in the RADBER program, a pause is made in the computations in order to output the results of the full integration to $\rho = \rho_A$. The format of this primary output depends upon the parameters and geometry under consideration as indicated in Table 1. In all cases the guessed values for j and J (A and B) in amps/cm^2 are listed as are the values found for r_S and r_A in centimeters as well as the values of the electric potential and electric field at $\rho = \rho_A$ in volts and volts/cm respectively. Depending upon the geometry being studied, $W(\rho_A)$ or $W'(\rho_A)$ may be listed along with the value it must have in a true steady state. The table thus created allows a quick evaluation of the merits of the (j,J) guesses tried for the given value of $W'(\rho_c)$. In addition, immediately following that table are listed complete radial profiles for the electric potential in volts and for the insulating magnetic field in gauss from ρ_c to ρ_A for the 11th, 12th, and 13th (j,J) guesses. These profiles provide invaluable information about how well-behaved the steady state conditions are for typical current density choices.

Having completed those pieces of data output, RADBER moves on to a comparison of the function values at the sheath boundary obtained by numerical integration on the cathode side and by analytic evaluation in the electron-free region on the anode side. The analytically obtained values are calculated in the subroutine, MATCH, using Eqs. (29)-(32) along with the values for ρ_S, X_S, and Y_S obtained in the subroutine, BOUND. These pairs of values to be matched at the sheath boundary are tabulated as the final block of output in a given $W'(\rho_c)$ cycle. The table heading clearly indicates which values should be compared to which (e.g., US1 to US2). It is useful to use this sheath boundary matching to fine-tune $(j,J,W'(\rho_c))$ guesses after some coarse fit to the chosen parameters has been

established in the $\rho = \rho_A$ matching table. The process suggested for this iterative improvement of guesses is illustrated by the examples given in Appendix B and Appendix C.

VI. CONCLUSIONS

The RADBER computer code which has resulted from the extensive theoretical, computational, and numerical efforts outlined above stands as a unique tool for analyzing numerous practical, high-voltage devices. It provides the experimenter with reliable predictions for electron and ion flow profiles as well as electric and magnetic field characteristics in coaxial, cylindrical geometry. Appendix A which follows this section provides a complete FORTRAN listing of the code. Appendix B illustrates the details of how the code is applied to a specific problem and how the iterative "shooting" technique is used to converge to the correct answer. The device chosen in this first sample case is a simple radial diode. Its treatment points out the danger of applying RADBER to a mixed axial-azimuthal insulation field. Finally, the much simpler problem of electron flow in a vacuum transmission line is treated for three different voltages in Appendix C. The solution has direct application to a power loss problem experienced in a more complicated coaxial geometry. Taken together, the two sample treatments explicitly demonstrate the versatility of the code.

ACKNOWLEDGMENTS

The authors are indebted to Shyke A. Goldstein and A. T. Drobot for numerous valuable discussions during the course of this work.

Appendix A

THE RADBER COMPUTER CODE

```
C
C
C-----------------------------------------------------------------------
C          THE RADBER PROGRAM
C-----------------------------------------------------------------------
C
      PARAMETER NDR=750
C
      LOGICAL LAZ,LCIN,LIONS
      INTEGER IFLAG(100)
      REAL*8 R,DR,RC,RANODE
C
      DIMENSION X(100,NDR),Y(100,NDR),XP(100,NDR),YP(100,NDR),URA(100)
     &    ,U(100,NDR),W(100,NDR),UU(100),WW(100),XX(100),YY(100)
     &    ,AC(100),BC(100),  SCA(100),SCB(100),SCC(100),SCD(100),
     &    SCE(100),SCF(100),SCG(100),SCH(100)
C
      COMMON /COEF/ A(100),B(100),RS(100),RA(100),AFLAG(100),
     &    R,DR,RC,RANODE,RINV,U0,B0,EBYMC2,EMRAT,C,GAPLEN
      COMMON /SWITCH/ LAZ,LCIN,LIONS
      COMMON /FIT/ UN(100),WN(100),XN(100),YN(100),UNM1(100),WNM1(100),
     &    XNM1(100),YNM1(100),RNM1(100),RSTAR(100),USTAR(100),WSTAR(100),
     &    XSTAR(100),YSTAR(100)
      COMMON /ITCHY/ SCRA(100),WS(100),US(100),ES(100)
C
      NAMELIST /GUESS/ AMIN,DELA,NA,BMIN,DELB,NB,FMIN,DELF,NF,I1,I2,I3
      NAMELIST/GIVEN/RC,RANODE,U0,B0,GAPLEN,CURCEN,ERROR,LAZ,LCIN,LIONS
C
C          IN NAMELIST 'GIVEN' -
C            GAPLEN, RC, AND RANODE ARE IN CENTIMETERS,
C            U0 IS IN VOLTS,
C            B0 IS IN GAUSS,
C            CURCEN IS IN AMPERES,
C            ERROR IS A DECIMAL FRACTION, AND
C            LAZ=.TRUE. FOR AN AZIMUTHAL INSULATION FIELD.
C            LCIN=.TRUE. FOR THE CATHODE AS THE CENTRAL CONDUCTOR
C            LIONS=.TRUE. FOR THE PRESENCE OF ION FLOW
C
C
C********** SUPPLY NEEDED CONSTANTS ******************************
C
      SIXINV=1.00/6.00
      C=2.9979E10
      PI=3.1416E0
      EMRAT=SQRT(1.6726E-24/(2.0*9.1095E-28))
      EBYMC2=4.8032E-10/(9.1095E-28*C*C)
C
C********** INITIALIZE AND SCALE THE VARIABLES ****************T*********
C
C*** FIRST READ IN THE DEFAULT PARAMETERS ***
C
      READ(5,GUESS)
      READ(5,GIVEN)
C
C*** THEN SUPPLY THE SPECIFIC VALUES ***
C
      READ(5,GUESS)
      READ(5,GIVEN)
      ASCALE = 8.0 * PI * RC * 3.0E9 / (C * B0)
      BSCALE = ASCALE * 0.5 * EMRAT
      RANODE = EBYMC2*B0*RANODE
      RC = EBYMC2*B0*RC
      U0 = EBYMC2*U0/3.0E2
      DR=(RANODE-RC)/DFLOAT(NDR)
      FACT=DR/24.0
      WRITE(6,GUESS)
      WRITE(6,GIVEN)
C
C****GENERATE THE CURRENT FLUX COEFFICIENTS **********************
C
      DO 2 I=1,NA
      AA= (AMIN+DELA*(I-1))*ASCALE
      DO 2 J=1,NB
      AC(I+NB*(J-1)) = AA
      BC(I+NB*(J-1)) =(BMIN+DELB*(J-1) )*BSCALE
 2    CONTINUE
```

```
C
C********** CALCULATE CORRECT U(RA) OR UP(RA) ********************
C
      IF(LAZ) GO TO 500
      UFAC=(RANODE**2-RC**2)/(2.0*RANODE)
      GO TO 501
 500  IF(LCIN) GO TO 502
      IF(LIONS) GO TO 503
      UFAC=B0*0.2*CURCEN*EBYMC2/RANODE
 501  DO 504 I=1,100
 504  URA(I)=UFAC
      GO TO 502
 503  UFAC=0.05*EBYMC2*C*B0*GAPLEN/(EMRAT*RANODE)
      DO 505 I=1,100
 505  UPA(I)=UFAC*B(I)
 502  CONTINUE
C
C********** ITERATE OVER CHOICES FOR CATHODE B-FIELD ******************
C
      IT=0
 400  IT=IT+1
      F=FMIN+DELF*(IT-1)
      R=RC
      IF(LAZ.AND.LCIN.AND..NOT.LIONS) F=0.2*CURCEN*EBYMC2/RC
      ICORR=0
      DO 1 I=1,100
      RS(I)=0.0
      RA(I)=0.0
      AFLAG(I)=1.0
      IFLAG(I)=0
      A(I)=AC(I)
      B(I)=BC(I)
 1    CONTINUE
C
C********** USE ANALYTIC APPROXIMATIONS TO GENERATE INITIAL **************
C*****!**** VALUES AT RC+DR            **********K**********************
C
      R=R+DR
      RINV=1.0/R
C
      CALL START(U,X,W,Y,F)
C
C********* TH ORDER RUNGA-KUTTA FOR STARTING VALUES ******************
C
      DO 4 I=1,4
C
      DO 5 J=1,100
      SCA(J)=DR*X(J,I)
 5    SCB(J)=DR*Y(J,I)
      DO 6 J=1,100
      SCC(J)=DR*(X(J,I)+SCA(J)*0.5)
 6    SCD(J)=DR*(Y(J,I)+SCB(J)*0.5)
      DO 7 J=1,100
      SCE(J)=DR*(X(J,I)+0.5*SCC(J))
 7    SCF(J)=DR*(Y(J,I)+0.5*SCD(J))
      DO 8 J=1,100
      SCG(J)=DR*(X(J,I)+SCE(J))
 8    SCH(J)=DR*(Y(J,I)+SCF(J))
C
      DO 9 J=1,100
      U(J,I+1)=U(J,I)+(SCA(J)+2.0*SCC(J)+2.0*SCE(J)+SCG(J))*SIXINV
 9    W(J,I+1)=W(J,I)+(SCB(J)+2.0*SCD(J)+2.0*SCF(J)+SCH(J))*SIXINV
C
      CALL PRIME(U(1,I),W(1,I),X(1,I),Y(1,I),XP(1,I),YP(1,I),I,IFLAG)
C
      DO 10 J=1,100
      SCG(J)=DR*XP(J,I)
 10   SCH(J)=DR*YP(J,I)
C
      R =R+0.5*DR
      RINV=1.0/R
C
      DO 11 J=1,100
      UU(J)=U(J,I)+0.5*SCA(J)
```

```
      UU(J)=U(J,I)+0.5*SCB(J)
      XX(J)=X(J,I)+0.5*SCG(J)
   11 YY(J)=Y(J,I)+0.5*SCH(J)
C
      CALL PRIME(UU,UU,XX,YY,SCA,SCB,I,IFLAG)
C
      DO 12 J=1,100
      SCA(J)=DR*SCA(J)
   12 SCB(J)=DR*SCB(J)
C
      DO 13 J=1,100
      UU(J)=U(J,I)+0.5*SCC(J)
      UU(J)=U(J,I)+0.5*SCD(J)
      XX(J)=X(J,I)+0.5*SCA(J)
   13 YY(J)=Y(J,I)+0.5*SCB(J)
C
      CALL PRIME(UU,UU,XX,YY,SCC,SCD,I,IFLAG)
C
      DO 14 J=1,100
      SCC(J)=DR*SCC(J)
   14 SCD(J)=DR*SCD(J)
C
      R=R+0.5*DR
      RINV=1.0/R
C
      DO 15 J=1,100
      UU(J)=U(J,I)+SCE(J)
      UU(J)=U(J,I)+SCF(J)
      XX(J)=X(J,I)+SCC(J)
   15 YY(J)=Y(J,I)+SCD(J)
C
      CALL PRIME(UU,UU,XX,YY,SCE,SCF,I,IFLAG)
C
      DO 16 J=1,100
      X(J,I+1)=X(J,I)+(SCG(J)+2.0*SCA(J)+2.0*SCC(J)+DR*SCE(J))*SIXINV
   16 Y(J,I+1)=Y(J,I)+(SCH(J)+2.0*SCB(J)+2.0*SCD(J)+DR*SCF(J))*SIXINV
C
    4 CONTINUE
C
      CALL PRIME(U(1,5),U(1,5),X(1,5),Y(1,5),XP(1,5),YP(1,5),5,IFLAG)
C
C*************************************************************
C     AT THIS POINT WE HAVE COMPLETE DATA FOR THE
C          FIRST FIVE POINTS.
C*************************5555**********************
C********** THE ADAMS-BASHFORTH-MOULTEN PREDICTOR-CORRECTOR
C
      DO 100 J=6,NDR
C
      R=R+DR
      RINV = 1.0/R
C
      DO 20 I=1,100
C
      X(I,J)=X(I,J-1)+FACT*(55.0*XP(I,J-1)-59.0*XP(I,J-2)
     &                +37.0*XP(I,J-3)-9.0*XP(I,J-4))
      Y(I,J)=Y(I,J-1)+FACT*(55.0*YP(I,J-1)-59.0*YP(I,J-2)
     &                +37.0*YP(I,J-3)-9.0*YP(I,J-4))
      U(I,J)=U(I,J-1)+FACT*(55.0*X(I,J-1)-59.0*X(I,J-2)
     &                +37.0*X(I,J-3)-9.0*X(I,J-4))
      W(I,J)=W(I,J-1)+FACT*(55.0*Y(I,J-1)-59.0*Y(I,J-2)
     &                +37.0*Y(I,J-3)-9.0*Y(I,J-4))
   20 CONTINUE
C
      CALL PRIME(U(1,J),W(1,J),X(1,J),Y(1,J),XP(1,J),YP(1,J),J,IFLAG)
C
C********** THE CORRECTOR
C
  101 CONTINUE
C
      DO 40 I=1,100
      SCA(I)=U(I,J-1)+FACT*(9.0*X(I,J)+19.0*X(I,J-1)
     &                -5.0*X(I,J-2)+X(I,J-3))
      SCB(I)=W(I,J-1)+FACT*(9.0*Y(I,J)+19.0*Y(I,J-1)
     &                -5.0*Y(I,J-2)+Y(I,J-3))
   40 CONTINUE
```

```
      DO 30 I=1,100
      X(I,J)=X(I,J-1)+FACT*(9.0*XP(I,J)+19.0*XP(I,J-1)
     &                -5.0*XP(I,J-2)+XP(I,J-3))
      Y(I,J)=Y(I,J-1)+FACT*(9.0*YP(I,J)+19.0*YP(I,J-1)
     &           -5.0*YP(I,J-2)+YP(I,J-3))
 30   CONTINUE
C
      CALL PRIME(SCA, SCB, X(1,J),Y(1,J),XP(1,J),YP(1,J),J,IFLAG)
C
C********** ERROR CHECK
C
      ICORR=ICORR+1
      IF(ICORR.GT.1000) GO TO 102
      DO 41 I=1,100
      SCC(I)=ABS((U(I,J)-SCA(I))/U(I,J))
 41   SCD(I)=ABS((W(I,J)-SCB(I))/W(I,J))
      DO 42 I=1,100
      U(I,J)=SCA(I)
 42   W(I,J)=SCB(I)
      DO 43 I=1,100
      IF(SCC(I).LT.ERROR) GO TO 43
      GO TO 101
 43   CONTINUE
      DO 44 I=1,100
      IF(SCD(I).LT.ERROR) GO TO 44
      GO TO 101
 44   CONTINUE
C
 100  CONTINUE
C
 102   CONTINUE
C
C*** USE ANALYTIC FIT AT SHEATH BOUNDARY ****************************
C
      DRSING=SNGL(DR)
      DO 601 I=1,100
      IF((DR*RS(I)).GE.(DR*RA(I))) GO TO 603
      GO TO 600
 603  IF(RA(I).EQ.0.0) GO TO 600
 602  UN(I)=1.0
      WN(I)=1.0
      XN(I)=0.0
      YN(I)=DRSING/ABS(DRSING)
      UNM1(I)=1.0
      WNM1(I)=1.0
      XNM1(I)=0.0
      YNM1(I)=YN(I)
      RNM1(I)=SNGL(RC)
      GO TO 601
 600  IF(IFLAG(I).LE.7) GO TO 602
      UN(I)=U(I,IFLAG(I)-1)
      WN(I)=W(I,IFLAG(I)-1)
      XN(I)=X(I,IFLAG(I)-1)
      YN(I)=Y(I,IFLAG(I)-1)
      UNM1(I)=U(I,IFLAG(I)-2)
      WNM1(I)=W(I,IFLAG(I)-2)
      XNM1(I)=X(I,IFLAG(I)-2)
      YNM1(I)=Y(I,IFLAG(I)-2)
      RNM1(I)=SNGL(RC+DR*(IFLAG(I)-2))
 601  CONTINUE
C
      CALL BOUND(DRSING,AC,BC,U0,5)
C
C*** SCALE SELECTED VARIABLES INTO CGS UNITS ******************
C
      USCA=3.0E2/EBYMC2
      RSCA=1.0/(B0*EBYMC2)
      DO 210 I=1,100
      A(I)= AC(I)/ASCALE
      B(I)= BC(I)/BSCALE
      RS(I)=RS(I)*RSCA
      RA(I)=RA(I)*RSCA
      U(I,NDR)=U(I,NDR)*USCA
      YP(I,NDR)=Y(I,NDR)*B0
```

```
      IF(LAZ) GO TO 210
      YP(I,NDR)=YP(I,NDR)+U(I,NDR)*B0/RANODE
  210 CONTINUE
C
C**************** THE OUTPUT ***********************************************
C
      BCATH = F*B0*0.001
      WRITE(6,999) BCATH
  999 FORMAT('1',///,20X,'FOR A MAGNETIC FIELD NEAR THE CATHODE OF',
     &   E18.5,' KILOGAUSS :',//)
      IF(LAZ) GO TO 201
      WRITE(6,1000)
 1000 FORMAT(3X,'I',9X,'A',11X,'B',14X,'RS',10X,'RA',11X,'E(RA)',
     &   7X,'U(RA)',11X,'U(RA)',7X,'URA',//)
      DO 200 I=1,100
  200 WRITE(6,1001) I,A(I),B(I),RS(I),RA(I),X(I,NDR),U(I,NDR),U(I,NDR)
     &   ,URA(I)
 1001 FORMAT(1X,I3,4(3X,2E12.4),/)
      GO TO 202
  201 IF(LCIN) GO TO 203
      WRITE(6,1002)
      DO 204 I=1,100
  204 WRITE(6,1001) I, A(I),B(I),RS(I),RA(I),X(I,NDR),U(I,NDR)
     &   ,YP(I,NDR),URA(I)
 1002 FORMAT(3X,'I',9X,'A',11X,'B',14X,'RS',10X,'RA',11X,'E(RA)'
     &   ,7X,'U(RA)',10X,'BT(RA)',6X,'BTRA',//)
      GO TO 202
  203 WRITE(6,1003)
      DO 205 I=1,100
  205 WRITE(6,1001) I,A(I),B(I),RS(I),RA(I),X(I,NDR),U(I,NDR)
 1003 FORMAT(2X,'I',12X,'A',16X,'B',15X,'RS',13X,'RA',12X,
     &   'E(RA)',8X,'U(RA)',//)
  202 CONTINUE
C
C********** CALCULATION OF SAMPLE B-FIELD PROFILES
C
      IF(LAZ) GO TO 251
      R=RC
      DO 250 I=1,NDR
      R=R+DR
      RINV=1.0/R
      YP(1,I)=(Y(I1,I)+U(I1,I)*RINV) * B0
      YP(2,I)=(Y(I2,I)+U(I2,I)*RINV) * B0
  250 YP(3,I)=(Y(I3,I)+U(I3,I)*RINV) * B0
      GO TO 253
  251 CONTINUE
      DO 252 I=1,NDR
      YP(1,I) = B0 *  Y(I1,I)
      YP(2,I) = B0 *  Y(I2,I)
  252 YP(3,I) = B0 *  Y(I3,I)
  253 CONTINUE
C
C*** SCALING OF THE POTENTIAL ***********************************
C
      DO 260 I=1,NDR
      U(I1,I) = U(I1,I) * USCA
      U(I2,I) = U(I2,I) * USCA
  260 U(I3,I) = U(I3,I) * USCA
C
      WRITE(6,1006) I1,I2,I3
 1006 FORMAT(1X,/////,1X,'PHI AND B-FIELD PROFILES FOR (A,B) CHOICES',
     &   I4,',',I4,', AND',I4,'  .',///)
C
      DO 300 I=1,NDR,2
  300 WRITE(6,1005) I,U(I1,I),YP(1,I),U(I2,I),YP(2,I),U(I3,I),YP(3,I)
 1005 FORMAT(1X,I3,3(3X,2E14.5))
C
C*** COMPARE VALUES AT ELECTRON SHEATH BOUNDARY ******************
C
      CALL MATCH(RSTAR,URA,YSTAR,XSTAR,BC)
C
      WRITE(6.1010)
```

```
 1010 FORMAT(1X,/////,1X,'MATCHING VALUES AT SHEATH BOUNDARY',//,
     &    3X,'I',9X,'RS',13X,'US1',8X,'US2',12X,'ES1',
     &    8X,'ES2',12X,'US1',9X,'YS1',9X,'US2',//)
C
C*** SCALE RSTAR INTO CENTIMETERS ***********************555*
C
      DO 650 I=1,100
  650 RS(I)=RSTAR(I)*RSCA
C
      DO 700 I=1,100
  700 WRITE(6,1004) I,RS(I),USTAR(I),US(I),XSTAR(I),ES(I),
     &               USTAR(I),YSTAR(I),US(I)
C
 1004 FORMAT(1X,I3,2X,E12.4,2(3X,2E12.4),3X,3E12.4,/)
      IF(IT.LT.NF) GO TO 400
C
      STOP
C
      END



C
C
C
C----------------------------------------------------------------------
C           SUBROUTINE BOUND
C----------------------------------------------------------------------
C
      SUBROUTINE BOUND(DR,A,B,U0,ITER)
C
      LOGICAL LAZ,LCIN,LIONS
C
      DIMENSION A(100),B(100),R(100),SCR1(100)
C
      COMMON /FIT/ UN(100),UN(100),XN(1C0),YN(100),UNM1(100),UNM1(100),
     &    XNM1(100),YNM1(100),RNM1(100),RSTAR(100),USTAR(100),USTAR(100),
     &    XSTAR(100),YSTAR(100)
      COMMON /SWITCH/ LAZ,LCIN,LIONS
      COMMON /ITCHY/ A1(100),B1(100),A2(100),B2(100)
C
      EPS=1.0
      IF(LAZ) EPS=0.0
      F = 1.0
      IF(.NOT.LCIN) F=-1.0
C
C*** MAKE ZEROETH-ORDER GUESSES **************************************
C
      DO 1 I=1,100
      R(I)=DR
      USTAR(I)=UN(I)
      USTAR(I)=UN(I)
      XSTAR(I)=XN(I)
    1 YSTAR(I)=YN(I)
C
C*** ITERATE FOR SOLUTIONS *******************************************
C
      DO 2 IT=1,ITER
C
C*** CALCULATE A1 AND B1 ***
C
      DO 3 I=1,100
      A2(I)=F*4.0*A(I)/(3.0*(R(I)+RNM1(I)))
    3 B2(I)=F*(2.*USTAR(I)*YSTAR(I)-2.*XSTAR(I)*(1.+USTAR(I)))
C
      DO 20 I=1,100
      IF(B2(I).GT.0.0) GO TO 20
      B2(I)=1.0E20
   20 CONTINUE
C
      DO 4 I=1,100
      A1(I)= A2(I)*(1.0+USTAR(I))/SQRT(B2(I))
```

```
 4    B1(I)= A2(I)*USTAR(I)/SQRT(B2(I))
C
C*** CHECK FOR NEGATIVE VALUES OF 'USTAR' **********************
C
      DO 30 I=1,100
      IF(USTAR(I).GT.0.0.AND.USTAR(I).LT.U0) GO TO 30
      USTAR(I)= (1.0E-3)*U0
 30   CONTINUE
C
C*** CALCULATE R-CORRECTED ***
C
      DO 5 I=1,100
      A2(I)= SQRT(USTAR(I)*(2.0+USTAR(I)))
  5   B2(I)= 1.0 + USTAR(I)
C
      DO 6 I=1,100
  6   RSTAR(I)= (A2(I)*(1.0+UNM1(I))-UNM1(I)*B2(I)) /
     &          (YSTAR(I)*B2(I) - XSTAR(I)*A2(I))
C
      DO 14 I=1,100
 14   IF((RSTAR(I)*F).GE.0.0) R(I)=RSTAR(I)
C
C*** CALCULATE A2 AND B2 ***
C
      DO 7 I=1,100
  7   SCR1(I)=-0.5/(R(I)+RNM1(I))
C
      DO 8 I=1,100
      A2(I)=SCR1(I)*(XSTAR(I)+B(I)/SQRT(U0-USTAR(I)))
  8   B2(I)=SCR1(I)*(YSTAR(I)+2.0*EPS*USTAR(I)*SCR1(I))
C
C*** CORRECT THE PREDICTED VALUES ***
C
      DO 9 I=1,100
      XSTAR(I)=XNM1(I)+1.5*A1(I)*SQRT(F*R(I))+2.0*A2(I)*R(I)
  9   YSTAR(I)=YNM1(I)+1.5*B1(I)*SQRT(F*R(I))+2.0*B2(I)*R(I)
C
      DO 10 I=1,100
      USTAR(I)=UNM1(I)+R(I)*(XSTAR(I)-A1(I)*SQRT(F*R(I))-A2(I)*R(I))
 10   USTAR(I)=UNM1(I)+R(I)*(YSTAR(I)-B1(I)*SQRT(F*R(I))-B2(I)*R(I))
C
  2   CONTINUE
C
      DO 12 I=1,100
 12   RSTAR(I)=RNM1(I)+R(I)
C
      RETURN
C
      END
C
C
C
C-----------------------------------------------------------------------
C          SUBROUTINE PRIME
C-----------------------------------------------------------------------
C
      SUBROUTINE PRIME(U,W,X,Y,XP,YP,IT,IFLAG)
C
      DIMENSION S(100),U(100),W(100),X(100),Y(100),XP(100),YP(100)
C
      COMMON /ITCHY/SCA(100),SCB(100),SCC(100),SCD(100)
      COMMON /COEF/ A(100),B(100),RS(100),RA(100),AFLAG(100),
     &    R,DR,RC,RANODE,RINV,U0,B0,EBYMC2,EMRAT,C,GAPLEN
      COMMON /SWITCH/ LAZ,LCIN,LIONS
C
      LOGICAL LAZ,LCIN,LIONS
      INTEGER IFLAG(100)
      REAL*8 R,DR,RC,RANODE
```

```
C
C********** FIND THE ELECTRON SHEATH RADIUS ****************************
C
      DO 1 I=1,100
 1    S(I)=2.0*U(I)+(U(I)+U(I))*(U(I)-U(I))
      DO 2 I=1,100
      IF(S(I).GT.1.0E-8) GO TO 2
      S(I)=1.0
      A(I)=0.0
      IF(IFLAG(I).EQ.0) IFLAG(I)=IT
 2    CONTINUE
C
      DO 7 I=1,100
 7    SCB(I)=A(I)+RS(I)
C
      DO 3 I=1,100
      IF(SCB(I).NE.0.0) GO TO 3
      RS(I)=R
 3    CONTINUE
C
C********** FIND THE 'ANODE RADIUS' ************************************
C
      DO 4 I=1,100
      IF(U(I).LT.U0) GO TO 4
      A(I)=0.0
      B(I)=0.0
      AFLAG(I)=0.0
      X(I)=0.0
      Y(I)=0.0
 4    CONTINUE
C
      DO 5 I=1,100
 5    SCA(I)=AFLAG(I)+RA(I)
C
      DO 6 I=1,100
      IF(SCA(I).NE.0.0) GO TO 6
      RA(I)=R
 6    CONTINUE
C
      DO 10 I=1,100
 10   SCA(I)= 1.0/SQRT(S(I))
      DO 11 I=1,100
 11   SCB(I)=A(I)*SCA(I)
      DO 12 I=1,100
      XP(I)=SCB(I)*(1.0+U(I))
 12   YP(I)=SCB(I)*U(I)
      DO 13 I=1,100
 13   SCA(I) = U0-U(I)
      DO 14 I=1,100
      IF(SCA(I).GT.0.0) GO TO 14
      SCA(I)=1.0
 14   CONTINUE
      DO 15 I=1,100
 15   SCC(I)=1.0/SQRT(SCA(I))
      DO 16 I=1,100
 16   SCA(I)=XP(I)-B(I)*SCC(I)
      DO 17 I=1,100
 17   SCB(I) = YP(I)
      IF(LAZ) GO TO 19
      DO 18 I=1,100
 18   SCB(I)=SCB(I)+AFLAG(I)*U(I)*RINU
 19   CONTINUE
      DO 20 I=1,100
      SCC(I)=SCA(I)-X(I)
 20   SCD(I)=SCB(I)-Y(I)
      DO 21 I=1,100
      XP(I)=SCC(I)*RINU
 21   YP(I)=SCD(I)*RINU
C
      RETURN
C
      END
```

```
C
C
C
C-----------------------------------------------------------------------
C          SUBROUTINE MATCH
C-----------------------------------------------------------------------
C
      SUBROUTINE MATCH(RSTAR,URA,YSTAR,XSTAR,BC)
C
      LOGICAL LAZ,LCIN,LIONS
      REAL*8 R,DR,RC,RANODE
C
      COMMON /COEF/ A(100),B(100),RS(100),RA(100),AFLAG(100),
     &              R,DR,RC,RANODE,RINV,U0,B0
      COMMON /SWITCH/ LAZ,LCIN,LIONS
      COMMON /ITCHY/ SCA(100),SCB(100),SCC(100),SCD(100)
C
      DIMENSION RSTAR(100),URA(100),YSTAR(100),XSTAR(100),
     &          BC(100),RAT(100),RATINV(100),G(100),BETA(100),
     &          BETAP(100)
C
C*** DETERMINE NEEDED CONSTANTS ********************************
C
      RASING=SNGL(RANODE)
      DO 1 I=1,100
      RAT(I)=RASING/RSTAR(I)
 1    G(I)=1.0
      DO 2 I=1,100
 2    RATINV(I)=1.0/RAT(I)
      DO 3 I=1,100
      IF(RATINV(I).GT.0.0) G(I)=ALOG(RATINV(I))
 3    CONTINUE
C
C*** MATCH THE MAGNETIC VARIABLE ********************************
C
      IF(LAZ) GO TO 4
C
      DO 5 I=1,100
 5    SCA(I)= 2.0*URA(I) - YSTAR(I)*(RASING-RSTAR(I)*RATINV(I))
      DO 6 I=1,100
      IF(RAT(I).NE.1.0) GO TO 7
      GO TO 6
 7    SCB(I) = SCA(I)/ (RAT(I)+RATINV(I))
 6    CONTINUE
      GO TO 8
C
 4    CONTINUE
      DO 9 I=1,100
 9    SCB(I) = URA(I)*RAT(I)/B0
C
 8    CONTINUE
C
C*** MATCH THE ELECTRICAL VARIABLES *****************************
C
      IF(.NOT.LIONS) GO TO 20
C
      DO 10 I=1,100
      BETA(I) = G(I)*( 1.0 - G(I)*( 0.400 - G(I)*( 9.1666E-2
     &   - G(I)*( 1.4242E-2 - G(I)*( 1.6793E-3 - G(I)*( 1.6122E-4
     &   - G(I)*( 1.2935E-5 - G(I)*( 8.8769E-7 - G(I)*( 5.4619E-8
     &   - G(I)*( 2.9484E-9 - G(I)*( 1.3603E-10 - G(I)*( 7.1101E-13
     &   - G(I)*( 2.6644E-13 + G(I)* 1.2526E-15))))))))))))
 10   CONTINUE
C
      DO 11 I=1,100
      BETAP(I) = ( 1.0 - G(I)*( 0.8 -G(I)*( 2.75E-1 - G(I)*(
     &   5.6968E-2 - G(I)*( 8.3964E-3 - G(I)*( 9.6733E-4
     &   - G(I)*( 9.0544E-5 - G(I)*( 7.1015E-6 - G(I)*( 4.9157E-7
     &   - G(I)*( 2.9484E-8 - G(I)*( 1.4963E-9 - G(I)*( 8.5321E-12
     &   - G(I)*( 3.4637E-12 + G(I)* 1.7536E-14))))))))))))/RSTAR(I)
 11   CONTINUE
```

```
C
      DO 12 I=1,100
 12   SCC(I) = U0 - (ABS(9.0*RSTAR(I)*BETA(I)*BETA(I)*BC(I))/4.0)
     &                **(2.0/3.0)
      DO 13 I=1,100
 13   SCD(I)= -(2.0/3.0)*(U0 - SCC(I))*(1.0/RSTAR(I)
     &          + 2.0*BETAP(I)/BETA(I))
      GO TO 14
C
 20    CONTINUE
C
      DO 15 I=1,100
 15   IF(RAT(I).GT.0.0) G(I)=ALOG(RAT(I))
      DO 16 I=1,100
 16   SCC(I) = U0 - XSTAR(I)*RSTAR(I)*G(I)
C
 14   RETURN
C
      END
```

Appendix B

SAMPLE SOLUTION FOR A RADIAL DIODE

In order to provide an example of the iterative "shooting" technique solution process, the radial diode depicted in Fig. 6 was modeled. Two megavolt operation of such a geometry should make the case interesting to those in the light ion beam research area. The desired configuration was specified by the following choice of variables:

a. LAZ = .FALSE.,

b. LCIN = .TRUE.,

c. LIONS = .TRUE.,

d. RC = 5.0,

e. RANODE = 5.5,

f. UØ = 2.0E6, and

g. BØ = 2.0E4.

As for the numerical factors, NDR was left at 500 and ERROR was chosen as 0.02.

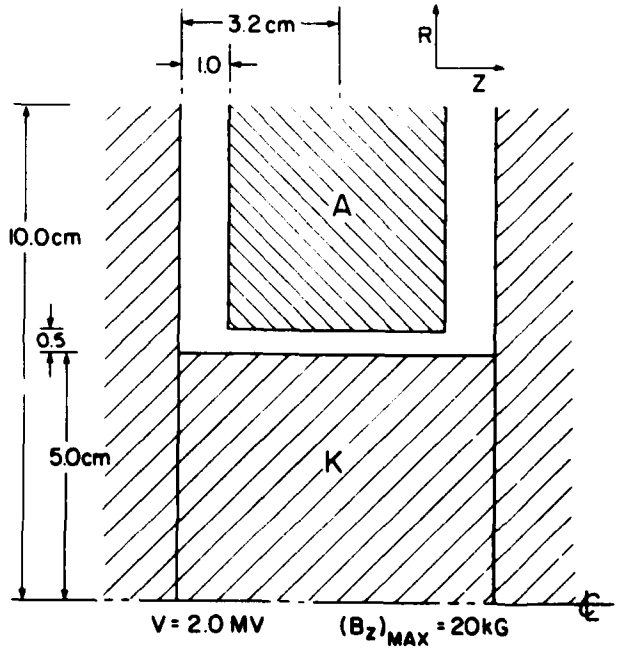

Fig. 6 — The radial diode test case

A quasi-static computer simulation of this diode has been completed[25] and the numerical results indicate an electron current density at the cathode of approximately 3.8×10^4 amps/cm^2 with a complementary ion current density of about 1.3×10^4 amps/cm^2. Due to the geometric electric field enhancement at the anode surface, it can be assumed that this ion current is too high. In the simulation, the axial magnetic field strength at the cathode surface was found to go slightly negative. Such field reversal cannot be expected if the electron and ion currents are significantly reduced. Given the high voltages of this test case, the approximate solutions presented in Figs. 3 and 4 do not provide any additional assistance in choosing reasonable guesses. As a first test for RADBER, therefore, it was decided to search the following parameter ranges:

(a) $(B_z)_{\text{cathode}} = 4$, 5, 6, 7, and 8 kilogauss.

(b) Ten equispaced values of $2.0 \times 10^4 \leqslant j \leqslant 4.25 \times 10^4$ amps/cm^2.

(c) Ten equispaced values of $0.3 \times 10^4 \leqslant J \leqslant 0.75 \times 10^4$ amps/cm^2.

In examining the numerical results from the program it is important to note that in cases such as this where the electron sheath boundary will lie close to the anode surface, the matching of values at $\rho = \rho_A$ is extremely unreliable due to the sharp discontinuities in U'' and W'' at $\rho = \rho_S$. As a general rule, therefore, one must perform the matching tests at $\rho = \rho_S$. After good matches are found there, the corresponding tables for $\rho = \rho_A$ may or may not add corroboration but they can never be used to overrule the ρ_S test results. Similarly, the sample ϕ and B_z profiles are to be trusted completely only *inside* the electron sheath.

An examination of the matching results for this first parameter search yielded, as might be expected, only a few promising candidates. By far most of the values to be compared at $\rho = \rho_S$ differed by at least factors of two. From this mass of data, however, the best matches were extracted for presentation in Table 2. The closest fit seems to be reached for $(B_z)_{\text{cath}} = 7$ kG, $j = 2.75 \times 10^4$ and $J = 0.35 \times 10^4$. The next logical search region seems to be:

TABLE 2. SAMPLE RADIAL DIODE OUTPUT

BZ	JE	JI	(US)IN	(US)OUT	(XS)IN	(XS)OUT	(WS)IN	(WS)OUT
5.0	2.50	0.40	2.36	3.89	0.552	0.559	3.21	5.54
5.0	4.00	0.55	2.95	3.89	0.443	0.688	3.82	5.52
6.0	2.70	0.40	2.85	3.76	0.703	0.956	3.72	5.25
6.0	3.50	0.45	3.36	3.91	0.532	0.340	4.25	5.58
7.0	2.25	0.30	3.23	3.87	0.855	0.612	4.11	5.44
7.0	2.75	0.35	3.48	3.86	0.772	0.694	4.36	5.41
7.0	3.50	0.40	3.74	3.85	0.293	0.776	4.63	5.38
8.0	2.50	0.30	3.66	3.73	0.906	0.871	4.55	5.08

WHERE IN THIS TABLE AS WELL AS IN TABLES 3, 4, AND 5:
BZ IS IN KILOGAUSS,
JE AND JI ARE IN UNITS OF 10,000 AMP/CMSQ, AND
US, XS, AND WS ARE ALL DIMENSIONLESS.

(a) $(B_z)_{cath}$ = 6.5, 7.0, and 7.5 kG.

(b) Ten equispaced values for $2.0 \times 10^4 \leqslant j \leqslant 3.8 \times 10^4$.

(c) Ten equispaced values for $0.25 \times 10^4 \leqslant J \leqslant 0.43 \times 10^4$.

The RADBER-generated matching values at $\rho = \rho_S$ provided the results listed in Table 3. The best overall answers seem to be for $(B_z)_{cath} = 7.5$ kG, $j = 2.80 \times 10^4$, and $J = 0.33 \times 10^4$. For those parameters, the worst match occurs for W_S. However, the jump in those values of W_S compared to their neighbors in the table suggests that the program is searching in a sensitive region of parameter space. Such "sensitivity" often implies that one is close to the correct answer in the search. To further delineate the correct range, it seems reasonable to check adjacent $(B_z)_{cath}$ values. For the third test search, therefore, the following ranges are chosen:

(a) $(B_z)_{cath} = 7.25$, 7.50, 7.75, and 8.00 kG.

(b) Ten equispaced values of $1.7 \times 10^4 \leqslant j \leqslant 3.5 \times 10^4$.

(c) Ten equispaced values of $0.25 \times 10^4 \leqslant J \leqslant 0.43 \times 10^4$.

TABLE 3. SAMPLE RADIAL DIODE OUTPUT

BZ	JE	JI	(US)IN	(US)OUT	(XS)IN	(XS)OUT	(WS)IN	(WS)OUT
6.5	2.00	0.29	2.98	3.89	0.790	0.526	3.85	5.51
6.5	2.20	0.31	2.81	3.86	0.788	0.635	3.68	5.42
6.5	3.00	0.39	3.38	3.89	0.688	0.604	4.26	5.50
6.5	3.20	0.41	3.43	3.86	0.643	0.732	4.32	5.43
7.0	2.00	0.29	2.76	3.60	0.850	0.981	3.63	4.95
7.0	2.20	0.31	2.94	3.66	0.860	0.962	3.81	5.03
7.0	2.40	0.33	3.09	3.69	0.857	0.959	3.97	5.08
7.0	2.60	0.35	3.21	3.70	0.841	0.975	4.09	5.09
7.0	2.80	0.35	3.55	3.89	0.732	0.559	4.44	5.50
7.0	3.00	0.37	3.60	3.86	0.674	0.698	4.49	5.42
7.5	2.00	0.27	3.06	3.67	0.938	0.890	3.93	5.01
7.5	2.20	0.29	3.23	3.71	0.934	0.884	4.11	5.07
7.5	2.40	0.31	3.36	3.72	0.914	0.899	4.24	5.09
7.5	2.60	0.33	3.46	3.71	0.880	0.934	4.35	5.08
7.5	2.80	0.33	3.75	3.87	0.667	0.641	4.65	5.43
7.5	2.80	0.35	3.54	3.69	0.835	0.988	4.43	5.03
7.5	3.00	0.35	3.78	3.82	0.530	0.784	4.67	5.31

The best matches are listed in Table 4. Clearly the most tantalizing results are those for the 8.0 kilogauss case. For that fixed value of $(B_z)_{cath}$ a close match for each of the three variables tested can be *found within the given* (j,J) matrix. More importantly, all of the matches fall on the line $j = 2.10 + 10\,(J - 0.27) = 10J - 0.60$. Two possibilities suggest themselves; either *the* solution falls on a similar line for an adjacent magnetic field value or it lies on an adjacent (j,J)-line unresolved by the coarse mesh but at the same field value. The former alternative will be tested first by examining the same (j,J) mesh for the values, $(B_z)_{cath} = 7.9, 8.1, 8.2, 8.3, 8.4, 8.5$. The major results are listed in Table 5. The coalescence of circled solutions indicates a finer scale search in the region delineated by:

(a) $(B_z)_{cath} = 8.3, 8.4, 8.5, 8.6, 8.7$ kG.

(b) Ten equispaced values of $1.65 \times 10^4 \leqslant j \leqslant 2.55 \times 10^4$.

(c) Ten equispaced values of $0.225 \times 10^4 \leqslant J \leqslant 0.315 \times 10^4$

No tabulated results are necessary for this run since a "hit" was scored in the $\rho = \rho_S$ matching results for the parameter combination $(B_z)_{cath} = 8.7$ kG, $j = 2.25 \times 10^4$ amps/cm^2, and $J = 0.275 \times 10^4$

TABLE 4. SAMPLE RADIAL DIODE OUTPUT

BZ	JE	JI	(US)IN	(US)OUT	(XS)IN	(XS)OUT	(WS)IN	(WS)OUT
7.25	2.10	0.29	3.00	3.66	0.899	0.928	3.87	5.02
7.25	2.30	0.31	3.16	3.70	0.895	0.924	4.04	5.07
7.25	2.50	0.33	3.29	3.71	0.878	0.939	4.17	5.09
7.25	2.90	0.35	3.68	3.86	0.678	0.671	4.57	5.42
7.25	3.10	0.35	3.81	3.91	0.321	0.338	4.70	5.58
7.25	3.10	0.37	3.70	3.82	0.605	0.807	4.60	5.32
7.50	2.50	0.31	3.56	3.83	0.859	0.723	4.45	5.33
7.50	2.70	0.33	3.63	3.81	0.801	0.792	4.52	5.27
7.50	2.90	0.33	3.83	3.89	0.459	0.501	4.73	5.52
7.50	2.90	0.35	3.68	3.77	0.734	0.879	4.57	5.19
7.50	3.10	0.35	3.83	3.85	0.366	0.726	4.72	5.37
7.50	3.10	0.37	3.71	3.73	0.662	0.975	4.60	5.09
7.50	3.30	0.37	3.82	3.78	0.288	0.888	4.71	5.22
7.50	2.90	0.39	3.22	3.26	0.908	1.374	4.09	4.40
7.50	3.10	0.39	3.53	3.52	0.813	1.207	4.41	4.75
7.75	2.10	0.27	3.29	3.72	0.972	0.841	4.17	5.07
7.75	2.30	0.29	3.43	3.73	0.950	0.855	4.32	5.10
7.75	2.50	0.31	3.54	3.73	0.910	0.891	4.43	5.08
7.75	2.70	0.31	3.83	3.87	0.627	0.610	4.72	5.43
7.75	2.70	0.33	3.62	3.70	0.856	0.947	4.51	5.04
7.75	2.90	0.33	3.84	3.82	0.517	0.762	4.74	5.30
8.00	2.10	0.27	3.26	3.59	1.011	0.958	4.14	4.82
8.00	2.30	0.29	3.40	3.61	0.994	0.977	4.29	4.85
8.00	2.50	0.31	3.52	3.60	0.960	1.012	4.41	4.84
8.00	2.70	0.33	3.61	3.58	0.911	1.063	4.50	4.80
8.00	2.90	0.35	3.67	3.54	0.849	1.125	4.56	4.74
8.00	3.10	0.37	3.72	3.49	0.778	1.197	4.61	4.65
8.00	3.30	0.39	3.75	3.42	0.701	1.276	4.64	4.55

TABLE 5. SAMPLE RADIAL DIODE OUTPUT

BZ	JE	JI	(US)IN	(US)OUT	(XS)IN	(XS)OUT	(WS)IN	(WS)OUT
7.9	2.30	0.29	3.42	3.66	0.977	0.932	4.30	4.95
7.9	2.50	0.31	3.53	3.65	0.940	0.968	4.42	4.94
7.9	2.70	0.33	3.61	3.63	0.889	1.020	4.50	4.90
7.9	2.90	0.35	3.68	3.59	0.826	1.085	4.57	4.83
7.9	3.10	0.37	3.72	3.54	0.754	1.160	4.61	4.74
7.9	3.30	0.39	3.75	3.47	0.677	1.241	4.64	4.64
7.9	3.50	0.41	3.76	3.40	0.599	1.133	4.65	4.52
8.1	2.10	0.27	3.24	3.53	1.026	0.998	4.12	4.71
8.1	2.30	0.29	3.39	3.55	1.011	1.018	4.28	4.75
8.1	2.50	0.31	3.51	3.55	0.980	1.053	4.40	4.74
8.1	2.70	0.33	3.60	3.53	0.932	1.102	4.49	4.71
8.1	2.90	0.35	3.67	3.49	0.873	1.163	4.56	4.65
8.1	3.10	0.37	3.72	3.44	0.802	1.233	4.61	4.56
8.2	2.10	0.27	3.22	3.47	1.040	1.035	4.10	4.61
8.2	2.30	0.29	3.38	3.50	1.028	1.056	4.26	4.65
8.2	2.50	0.31	3.50	3.50	0.999	1.091	4.39	4.64
8.2	2.50	0.33	3.20	3.16	1.030	1.314	4.08	4.18
8.2	2.70	0.33	3.59	3.48	0.954	1.139	4.48	4.61
8.2	2.90	0.35	3.66	3.44	0.897	1.198	4.56	4.55
8.3	1.90	0.25	3.01	3.36	1.045	1.058	3.88	4.44
8.3	2.10	0.27	3.21	3.41	1.054	1.069	4.08	4.51
8.3	2.30	0.29	3.37	3.44	1.045	1.092	4.25	4.55
8.3	2.50	0.31	3.49	3.44	1.018	1.127	4.38	4.55
8.3	2.70	0.33	3.59	3.42	0.975	1.174	4.48	4.52
8.3	2.90	0.35	3.66	3.39	0.918	1.232	4.55	4.46
8.4	1.90	0.25	2.99	3.29	1.057	1.088	3.86	4.34
8.4	2.10	0.27	3.19	3.35	1.069	1.101	4.07	4.41
8.4	2.30	0.29	3.35	3.38	1.062	1.125	4.23	4.45
8.4	2.50	0.31	3.48	3.39	1.037	1.160	4.37	4.45
8.4	2.70	0.33	3.58	3.37	0.996	1.207	4.47	4.42
8.5	1.90	0.25	2.97	3.23	1.067	1.117	3.84	4.24
8.5	2.10	0.27	3.17	3.29	1.082	1.131	4.05	4.31
8.5	2.30	0.29	3.34	3.32	1.077	1.156	4.22	4.35
8.5	2.50	0.29	3.00	2.92	1.069	1.365	3.88	3.88
8.5	2.50	0.31	3.47	3.33	1.056	1.192	4.35	4.35

amps/cm^2. For that choice, RADBER found the following: $r_S = 5.445$, $(U_S)_{in} = 3.438$, $(U_S)_{out} = 3.381$, $(X_S)_{in} = 1.104$, $(X_S)_{out} = 1.096$, $(W_S)_{in} = 4.324$, and $(W_S)_{out} = 4.397$. It is interesting to note that the matching at $\rho = \rho_A$ yielded $r_S = 5.445$, $r_A = 5.497$, $E_A = -0.0053$, $\phi_A = 2.0$ MV, and $W_A = 5.435$. Only the value for W_A is significantly displaced from its proper value of 5.600. A final fine-tuning run is called for not so much to obtain better values for the parameter guesses but rather to obtain useable profiles for the quantities $\phi(r)$ and $B_z(r)$. For this final run, it was decided to pick:

(a) $(B_z)_{cath} = 8.675$, 8.700, and 8.725 kG.

(b) Ten equispaced values of $2.05 \times 10^4 \leqslant j \leqslant 2.50 \times 10^4$.

(c) Ten equispaced values of $0.255 \times 10^4 \leqslant J \leqslant 0.300 \times 10^4$.

The results of that run clearly indicate a best choice of parameters as $[(B_z)_{cath}, j, J)] = [8.725$ kG, 22.0 kA/cm^2, 2.75 kA/cm^2]. For that combination, matching at $\rho = \rho_S$ yielded $(U_S)_{in} = 3.306$, $(U_S)_{out} = 3.268$, $(E_S)_{in} = 1.116$, $(E_S)_{out} = 1.152$, $(W_S)_{in} = 4.188$, $(W_S)_{out} = 4.235$, and $r_S = 5.436$ cm. The percentage errors in each of the respective quantities are $\Delta_U = 1.2\%$, $\Delta_E = 3.2\%$, and $\Delta_W = 1.1\%$. Given the 2% error margin chosen for the predictor-corrector, it is mathematically pointless to seek a closer match. The radial profiles of the electrostatic potential and axial magnetic field values supplied by RADBER for that chosen solution are plotted in Fig. 7. Note that the nature of the B-field profile is qualitatively identical to those plotted by Ron, et al., (see Ref. 11). On the other hand, the E-field inferred from the curve of $\phi(r)$ in Fig. 7 sharply differs from that cited in the above journal article. The difference exists because the presence of ions was not treated in Ref. 11. Ion emission at the anode surface requires that the electric field strength go to zero there.

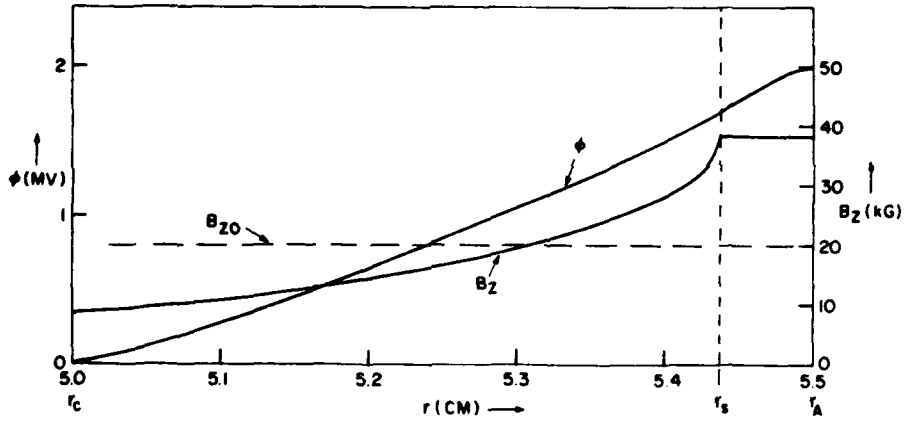

Fig. 7 — Profiles of ϕ and B_z in the A-K gap of the radial diode.

These RADBER results represent a very significant departure from the results of the full DIODE2D computer simulation of the radial diode under study. Instead of a slightly negative B_z at the cathode surface, RADBER predicts 8.725 kG. Instead of an electron current density of 38 kA/cm^2, RADBER finds 22 kA/cm^2. Finally, and most dramatically, we are left with only 2.75 kA/cm^2 of ion current density compared to DIODE2D's 13.0 kA/cm^2. These observed differences, however, may be attributed to two major causes:

(1) The electric field near the anode of the actual simulated radial diode is enhanced due to 2-D distortions which cannot be modeled by RADBER's one-dimensional treatment.

(2) The DIODE2D simulation accurately treated the azimuthal magnetic insulation present in the actual diode as well as the axial one. Given the currents of over a megampere flowing through the cathode shank, very large values of B_θ could be expected. This additional field component could easily have modified the results of the simple 1-D model by the degree shown. As an additional reference point, simple Child-Langmuir bi-polar analysis predicts an electron current density of just under 50 kA/cm^2 and a corresponding J of 1.2 kA/cm^2. It is interesting that both densities are off by factors of two from the RADBER results but in opposite directions.

In conclusion, therefore, RADBER, has given a reliable order-of-magnitude estimate for the current flow through the system. It also gives an investigator some appreciation for the degree to which combined axial and azimuthal insulation can modify a simple axial insulation prediction. Of course, RADBER can also be used to predict a purely azimuthal insulation result for this same diode in order to give even more insight into the overall physics of its operation. Such further studies would be valuable for specific diode designers.

Appendix C

SAMPLE SOLUTION FOR A VACUUM TRANSMISSION LINE

As part of the NRL Light Ion Fusion Research Program, high power diodes were tested for use as intense ion beam sources on the AURORA pulsed power generator at the Harry Diamond Laboratory. For these tests, the machine was operated in positive polarity so that the magnetically insulated coaxial feed line which transmits the power from the generator to the diode has a configuration qualitatively similar to that pictured in the lower half of Fig. 2. A significant difference, however, is that in the actual transmission line the outer conductor is conical rather than cylindrical. The specific geometry is drawn to scale in Fig. 8 with all dimensions given in centimeters. In recent ion diode runs on this device, clear evidence was found that significant amounts of electron current were impacting the outer circumference of the end of the inner conductor (anode). This could represent a significant loss of power that could have been usefully applied to the generation of ions in the diode instead. The 250 kiloamperes of current flowing through the anode stalk had been assumed to be quite sufficient for generating a strong enough azimuthal B-field to insulate any electron flow in the line. Apparently it may not be. The RADBER code can now be used to check the physics of the assumption.

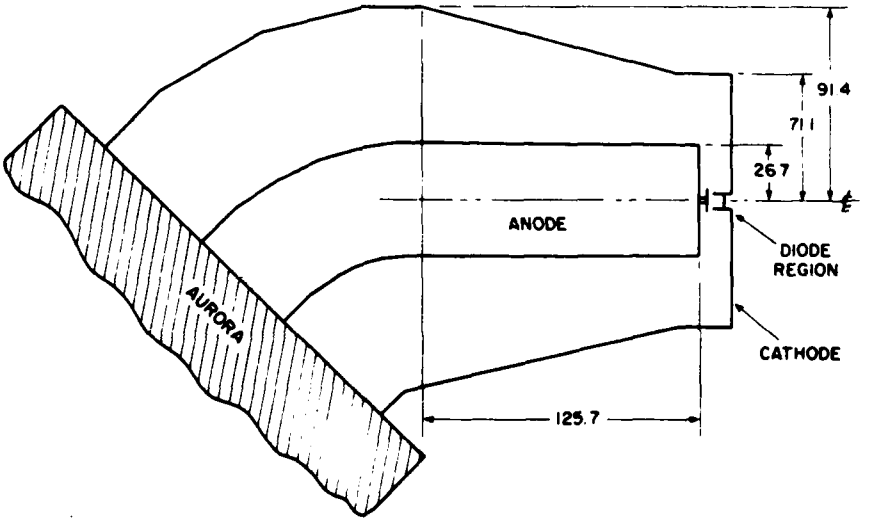

Fig. 8 — Modified AURORA magnetically insulated transmission line (MITL)

Quite differently from the case treated in Appendix B, the solutions at $\rho = \rho_S$ proved to be extremely erratic in the immediate vicinity of the true solution. This is to be expected judging from the sharp discontinuity in the slopes of both the electric field and the magnetic field for this case. On the other hand, the sharpness of the jumps in j space are a useful aide in pinpointing the solution after coarse tuning of the parameter guesses is accomplished through matching at $\rho = \rho_A$. For the 3 MV case, the correct steady state values for r_S, j, and $(B_\theta)_{cath}$ are 70.51 cm, 3.90 amp/cm^2, and 0.689 kG respectively. Similarly, for $\phi_0 = 4$ MV, they are 70.33 cm, 4.735 amp/cm^2, and 0.677 kG. Finally, for $\phi_0 = 5$ MV, the corresponding numbers are 70.03 cm, 6.315 amp/cm^2, and 0.663 kG. In Fig. 9 are plotted the profiles of ϕ and B_θ near the cathode for all three cases. Notice the pronounced discontinuity in the slope of each B_θ at its respective electron sheath boundary compared to the relatively smooth transition of ϕ across the same boundaries. In vacuum, the B_θ has a simple r^{-1} dependence while $\phi(r)$ is proportional to ln r.

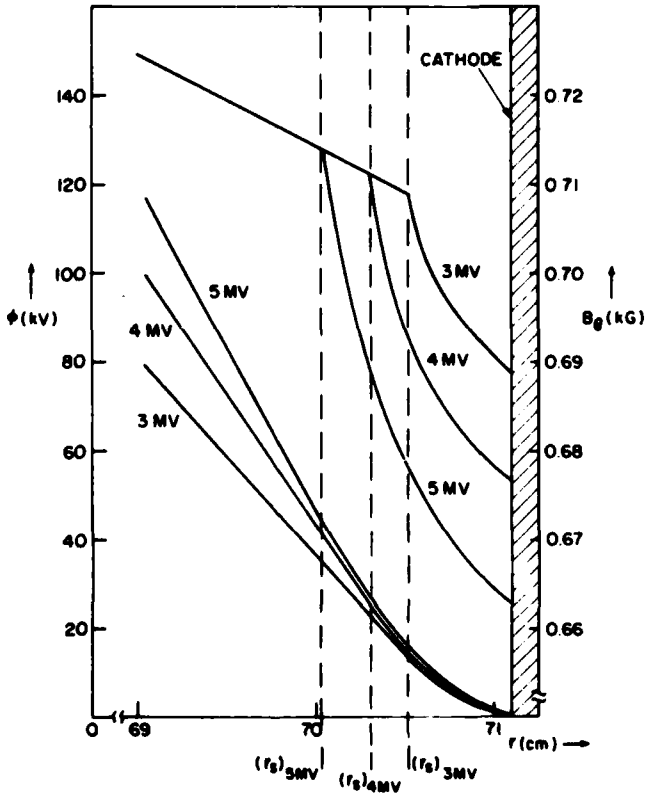

Fig. 9 — Profiles of ϕ and B_θ for the modified AURORA MITL

The weakest insulation can probably be expected near the end of the anode stalk where the damage was experimentally observed. Cylindrically coaxial equilibrium solutions will be sought for that region using RADBER for total voltages, ϕ_0, of 3.0, 4.0 and 5.0 mV. Assuming 250 kA of axial current in the anode stalk demands a vacuum B_θ of approximately 0.7032 kG at the lower cathode radius of 71.1 cm. That value will be used as the scale B-field, B_0. RADBER's numerical variables must then be set as follows:

a. LAZ = .TRUE.

b. LCIN = .FALSE.

c. LIONS = .FALSE.

d. ERROR = 0.01

e. RC = 71.1

f. RANODE = 26.7

g. UØ = 3.0E6, 4.0E6, and 5.0E6

h. BØ = 0.7032E3

i. CURCEN = 2.50E5.

This problem is somewhat simpler than that of the radial diode since no ion current is present. Thus, only two parameters, j and $(B_\theta)_{\text{cath}}$, must be guessed. Similarly, only two resultant parameters, U and $W' = Y$, must be matched at $\rho = \rho_S$ and $\rho = \rho_A$. As a starting point for parameter guesses, simple Child-Langmuir theory predicts about 6.2, 9.5 and 13.3 amps/cm^2 of emitted electron current density for $\phi_0 = 3.0$, 4.0 and 5.0 MV respectively. With such low values for j, relatively little departure from the vacuum B_θ of 0.70 kG can be expected. This in turn would lead to values of ρ_S very close to ρ_c. Because of that, finer resolution must be used in the numerical integration so that a value of $NDR = 750$ is chosen. The details of the numerical solution search process paralleling that used in Appendix B will not be given here. It is sufficient to note that the reduction of the work from a three-point to two-point shooting problem permitted convergence to a solution for each of the three voltages within three iterations of guesses.

These solutions indicate that there is very little to fear from power losses to electron flow in this feed line. The electron sheathes at the cathode surface are all on the order of only one centimeter thick compared to a radial anode-cathode separation of almost forty-five centimeters. The source of the experimentally-observed damage patterns is now believed to be some phenomenon associated with the plasma erosion switches used near the diode assembly.

REFERENCES

1. K.D. Bergeron, Phys. Fluids **20**, 688 (1977).

2. D.J. Johnson, et al., Phys. Rev. Lett. **42**, 610 (1979).

3. P. Dreike, et al., J. Appl. Phys. **47**, 85 (1976).

4. S. Humphries, Jr., et al., J. Appl. Phys. **47**, 2382 (1976).

5. M.Y. Wang and M.S. DiCapua, J. Appl. Phys. **51**, 5610 (1980).

6. B. Goplen, R.E. Clark, and S.J. Flint, Mission Research Corporation Report MRC/WDC-R-001 (1979).

7. A.A. Kolomenskii, E.G. Krastelev and B.N. Yablokov, Sov. Tech. Phys. Lett. **3**, 247 (1977).

8. J.D. Smith, Proc. 1st Inter. Conf. on Electron Beam Research and Technology **1**, 472 (1976).

9. R.N. Sudan and R.V. Lovelace, Phys. Rev. Lett. **31**, 1174 (1973).

10. R.V. Lovelace and E. Ott, Phys. Fluids **17**, 1263 (1974).

11. A. Ron, A.A. Mondelli and N. Rostoker, IEEE Trans. Plasma Science, PS-1, 85 (1973).

12. T.M. Antonsen, Jr. and E. Ott, Phys. Fluids **19**, 52 (1976).

13. J.M. Creedon, J. Appl. Phys. **46**, 2946 (1975).

14. O. Buneman, Proc. Camb. Philos. Soc. **50**, 77 (1954).

15. L. Brillouin, Phys. Rev. **67**, 260 (1945).

16. J. Swegle and E. Ott, Phys. Fluids **24**, 158 (1981).

17. I.D. Smith, P. D'A. Champney and J.M. Creedon, Proc. IEEE Inter. Pulsed Power Conf., Lubbock, Texas (1976).

18. A.T. Drobot, private communication.

19. Shyke A. Goldstein, J. Appl. Phys. **47**, 894 (1976).

20. S.D. Conte and Carl de Boor, *Elementary Numerical Analysis* 2d ed. (McGraw-Hill, New York, 1972), p. 338.

21. F.S. Acton, *Numerical Methods That Work* (Harper & Row, New York, 1970), p. 146.

22. I. Langmuir, Phys. Rev. Series 2 **2**, 450 (1913).

23. I. Langmuir and K.B. Blodgett, Phys. Rev. Series 2 **22**, 347 (1923).

24. *ASC FORTRAN Reference Manual*, Texas Instruments, Inc., Publication No. 930044-3 (1978).

25. R.J. Barker, S.A. Goldstein, and A.T. Drobot, Proc. IEEE Int. Conf. on Plasma Science, Montreal, Canada (1979).

DISTRIBUTION LIST JULY 1981

Director
Defense Intelligence Agency
Washington, DC 20301

Attn: DTICI Robert I. Rubenstein 1 copy

Defense Advanced Research Project Agency
1400 Wilson Blvd.
Arlington, VA 22209
Attn: J. Bayless 1 copy

Director
Defense Nuclear Agency
Washington, DC 20305

Attn:	FCPR	1 copy
	STVL	1 copy
	TISI Archives	1 copy
	TITL Tech. Library	3 copies
	J. Z. Farber (RAEV)	1 copy
	R. L. Gullickson (RAEV)	1 copy

Defense Technical Information Center
Cameron Station
5010 Duke Street
Alexandria, VA 22314

Attn: T. C. 12 copies

Under Sec'y of Defense for RSCH and ENGRG
Department of Defense
Washington, DC 20301

Attn: S&SS(OS) 1 copy

Chief
Livermore Division Fld Command DNA
Lawrence National Laboratory
P. O. Box 808
Livermore, CA 94550

Attn: FCPRL 1 copy

National Technical Information Service
U.S. Department of Commerce
5285 Port Royal Road
Springfield, VA 22161 — 24 copies

Commander
BMD System Command
P. O. Box 1500
Huntsville, AL 35807

Attn: SSC-TEN — 1 copy

DEP Chief of Staff for RSCH DEV & ACQ
Department of the Army
Washington, DC 20310

Attn: DAMA-CSM-N — 1 copy

Commander
Harry Diamond Laboratories
2800 Powder Mill Road
Adelphi, MD 20783
(CNWDI-INNER ENVELOPE: ATTN: DELHD-RBH)

Attn: DELHD-NP — 1 copy
DELHD-RCC J. A. Rosado — 1 copy
DRXDO-RBH P. A. Caldwell — 1 copy
DRXDO-RBH D. Schallhorn — 1 copy
DRXDO-TI Tech Lib. — 1 copy
S. Graybill — 1 copy

Commander
Picatinny Arsenal
Dover, NJ 07801

Attn: SMUPA ND-N-E — 1 copy

U. S. Air Force Office of Scientific Research
Physics Directorate
Bolling A.F.B., DC 20332

Attn: A. K. Hyder — 1 copy
M. A. Stroscio — 1 copy

Commander
U. S. Army Missile Command
Redstone Arsenal, AK 35809

Attn: Redstone Scientific Information CTR
DRCPM-PM-PE-EA — 1 copy

Commander
U. S. Army Nuclear Agency
7500 Backlick Road
Building 2073
Springfield, VA 22150

Attn: ATCN-W — 1 copy

Commander
U. S. Army Test and Evaluation COMD
Aberdeen Proving Ground, MD 21005

Attn: DRSTE-EL — 1 copy

Commander
Naval Electronic Systems CMD HQS
Washington, DC 20360

Attn: Code 5032 — 1 copy

Commanding Officer
Naval Intelligence Support Center
4301 Suitland Road - Building 5
Washington, DC 20390

Attn: NISC-45 — 1 copy

Naval Research Laboratory

Addressee: Attn: Name/Code	
Code 2628 - TIC-Distribution	25 copies
Code 4020 - J. Boris	1 copy
Code 6682 - D. Nagel	1 copy
Code 4700 - T. Coffey	26 copies
Code 4707 - J. Davis	1 copy
Code 4730 - S. Bodner	1 copy
Code 4740 - V. Granatstein	1 copy
Code 4760 - B. Robson	1 copy
Code 4761 - C. Kapetanakos	1 copy
Code 4770 - Branch Head	10 copies
Code 4770 - F. Young	1 copy
Code 4770 - S. Stephanakis	1 copy
Code 4771 - D. Mosher	10 copies
Code 4773 - G. Cooperstein	10 copies
Code 4790 - D. Colombant	1 copy
Code 4790 - I. Haber	1 copy
Code 4790 - M. Lampe	1 copy
On-Site Contractors:	
Code 4770 - R. Barker (Jaycor)	1 copy
Code 4770 - S. Goldstein (Jaycor)	1 copy
Code 4770 - R. Meger (Jaycor)	1 copy
Code 4770 - P. Ottinger (Jaycor)	1 copy
Code 4770 - F. Sandel (Jaycor)	1 copy
Code 4790 - A. Drobot (SAI)	1 copy

Officer-in-Charge
Naval Surface Weapons Center
White Oak, Silver Spring, MD 20910

Attn:	Code WR43	1 copy
	Code WA501 - Navy Nuc Prgms Off	1 copy

Chief of Naval Operations
Navy Department
Washington, DC 20350

Attn:	R. A. Blaise 604C4	1 copy

Commander
Naval Weapons Center
China Lake, CA 93555

Attn:	Code 533 Tech Lib.	1 copy

AF Weapons Laboratory, AFSC
Kirtland AFB, NM 87117

Attn:	CA	1 copy
	ELC	1 copy
	NT	1 copy
	SUL	1 copy
	DYP	1 copy
	J. Darrah	1 copy
	W.L. Baker	1 copy

HQ USAF/RD
Washington, DC 20330

Attn:	RDQSM	1 copy

Director
Joint Strat TGT Planning Staff JCS
OFFUTT AFB
Omaha, NB 68113

Attn:	JSAS	1 copy

SAMSO/DY
Post Office Box 92960
Worldway Postal Center
Los Angeles, CA 90009
(Technology)

Attn: DYS — 1 copy

SAMSO/IN
Post Office Box 92960
Worldway Postal Center
Los Angeles, CA 90009

Attn: IND MAJ D. S. Muskin — 1 copy

SAMSO/MN
Norton AFB, CA 92409
(Minuteman)

Attn: MNNH — 1 copy

SAMSO/SK
Post Office Box 92960
Worldway Postal Center
Los Angeles, CA 90009
(Space Comm Systems)

Attn: SKF P. H. Stadler — 1 copy

U. S. Department of Energy
Division of Inertial Fusion
Washington, DC 20545

Attn: G. Canavan — 1 copy
T. F. Godlove — 1 copy
S. L. Kahalas — 1 copy
R. L. Schriever — 1 copy

Argonne National Laboratory
9700 South Cass Avenue
Argonne, Illinois 60439

Attn: G. R. Magelssen — 1 copy
R. J. Martin — 1 copy

Brookhaven National Laboratory
Upton, NY 11973

Attn: A. F. Maschke — 1 copy

Lawrence Berkley Laboratory
Berkley, CA 94720

Attn: D. Keefe — 1 copy

Lawrence Livermore National Laboratory
P. O. Box 808
Livermore, CA 94550

Attn:	L-18	1 copy
	L-153	1 copy
	R. O. Bangerter	1 copy
	R. J. Briggs	1 copy
	E. P. lee	1 copy
	J. H. Nuckolls	1 copy
	S. S. Yu	1 copy
	Tech Info Dept. L-3	1 copy

Los Alamos National Laboratory
P. O. Box 1663
Los Alamos, NM 87545

Attn:	D. B. Henderson	1 copy
	R. B. Perkins	1 copy
	L. E. Thode	1 copy

National Science Foundation
Mail Stop 19
Washington, DC 20550

Attn: D. Berley — 1 copy

Sandia National Laboratories
P. O. Box 5800
Albuquerque, NM 87185

Attn:	J. R. Freeman / 4241	1 copy
	S. Humphries / 4253	1 copy
	D. J. Johnson / 4244	1 copy
	G. W. Kuswa / 4240	1 copy
	P. A. Miller / 4244	1 copy
	J. P. Vandevender / 4252	1 copy
	G. Yonas / 4200	1 copy
	Doc Con for 3141 Sandia RPT Coll	1 copy

AVCO Research and Systems Group
201 Lowell Street
Wilmington, MA 01887

Attn:	Research Lib. A830 Rm. 7201	1 copy

BDM Corporation, The
795 Jones Branch Drive
McLean, VA 22101

Attn:	Tech Lib.	1 copy

Bechtel Group, Inc.
P.O. Box 3965
San Francisco, CA 94119

Attn:	W. O. Allen	1 copy

Boeing Company, The
P. O. Box 3707
Seattle, WA 98124

Attn:	Aerospace Library	1 copy

Cornell University
Ithaca, NY 14850

Attn:	D. A. Hammer	1 copy
	R. N. Sudan	1 copy
	J. Maenchen	1 copy

The Dikewood Corporation
1613 University Blvd., NE
Alburquerque, NM 87102

Attn: L. Wayne Davis 1 copy

EG&G, Inc.
Albuquerque Division
P. O. Box 10218
Albuquerque, NM 87114

Attn: Technical Library 1 copy

Ford Aerospace & Communications Operations
Ford & Jamboree Roads
Newport Beach, CA 92663
(Formerly Aeronutronic Ford Corporation)

Attn: Tech Info Section 1 copy

General Electric Company
Space Division
Valley Forge Space Center
Goddard Blvd., King of Prussia
P. O. Box 8555
Philadelphia, PA 19101

Attn: J. C. Penden VFSC, Rm. 4230M 1 copy

General Electric Company
Tempo-Center for Advanced Studies
816 State Street (P. O. Drawer QQ)
Santa Barbara, CA 93102

Attn: DASIAC 1 copy

Grumman Aerospace Corporation
Bethpage, NY 11714

Attn: P. Suh 1 copy

Institute for Defense Analyses
400 Army-Navy Drive
Arlington, VA 22202

Attn: IDA Librarian R S. Smith — 1 copy

Ion Physics Corporation
South Beford Street
Burlington, MA 01803

Attn: H. Milde — 1 copy

IRT Corporation
P. O. Box 81087
San Diego, CA 92138

Attn: R. L. Mertz — 1 copy

JAYCOR, Inc.
205 S. Whiting Street
Alexandria, VA 22304

Attn: E. Alcaraz — 1 copy
J. Guillory — 1 copy
R. Hubbard — 1 copy
R. Sullivan — 1 copy
D. A. Tidman — 1 copy

JAYCOR, Inc.
11011 Torreyana Road
San Diego, CA 92121

Attn: E. Wenaas — 1 copy

Kaman Science Corporation
P. O. Box 7463
Colorado Springs, CO 80933

Attn: A. P. Bridges — 1 copy
D. H. Bryce — 1 copy
J. R. Hoffman — 1 copy
W. E. Ware — 1 copy

Lockheed Missiles and Space Co., Inc.
3251 Hanover Street
Palo Alto, CA 94304

Attn:	L. F. Chase	1 copy

Massachusetts Institute of Technology
Cambridge, MA. 02139

Attn:	R.C. Davidson	1 copy
	G. Bekefi	1 copy
	D. Hinshelwood	1 copy

Maxwell Laboratories, Inc.
9244 Balboa Avenue
San Diego, CA 92123

Attn:	R. W. Clark	1 copy
	A. C. Kolb	1 copy
	P. Korn	1 copy
	A. R. Miller	1 copy
	J. Pearlman	1 copy

McDonnell Douglas Corporation
5301 Bolsa Avenue
Huntington Beach, CA 92647

Attn:	S. Schneider	1 copy

Mission Research Corporation
1400 San Mateo Blvd. SE
Albuquerque, NM 87108

Attn:	B. B. Godfrey	1 copy

Mission Research Corporation-San Diego
P. O. Box 1209
LaJolla, CA 92038

Attn:	V.A.J. Van Lint	1 copy

Mission Research Corporation
735 State Street
Santa Barbara, CA 93101

Attn:	W. C. Hart	1 copy
	C. L. Longmire	1 copy

Northrop Corporation
Electronic Division
2301 West 120th Street
Hawthorne, CA 90250

Attn: V. R. DeMartino 1 copy

Northrop Corporation
Northrop Research and Technology Ctr.
3401 West Broadway
Hawthorne, CA 90205 1 copy

Physical Dynamics
P.O. Box 556
La Jolla, CA 92037

Attn: S. Jorna 1 copy

Physics International Co.
2700 Merced Street
San Leandro, CA 94577

Attn: J. Benford 1 copy
B. Bernstein 1 copy
G. Frazier 1 copy
R. Genuario 1 copy
E. B. Goldman 1 copy
R. Huff 1 copy
A. J. Toepfer 1 copy

Pulsar Associates, Inc.
11491 Sorrento Valley Blvd.
San Deigo, CA 92121

Attn: C. H. Jones, Jr. 1 copy

Princeton Plasma Physics Laboratory
James Forrestal Campus
P.O. Box 451
Princeton, N.J. 08540

Attn: R. Kulsrud 1 copy

Pulse Sciences, Inc.
1615 Broadway, Suite 610
Oakland, CA 94612

Attn:	I. Smith	1 copy
	P. Spence	1 copy
	S. Putman	1 copy

R&D Associates
P. O. Box 9695
Marina Del Rey, CA 90291

Attn:	W. R. Graham, Jr.	1 copy
	M. Grover	1 copy
	C. MacDonald	1 copy
	E. Martinelli	1 copy

R&D Associates
Suite 500
1401 Wilson Blvd.
Arlington, VA 22209

Attn: P. J. Turchi 1 copy

Science Applications, Inc.
P. O. Box 2351
LaJolla, CA 92038

Attn: J. Robert Beyster 1 copy

Spire Corporation
P. O. Box D
Bedford, MA 01730

Attn: R. G. Little 1 copy

SRI International
333 Ravenswood Avenue
Menlo Park, CA 94025

Attn: Setsuo Ddairiki 1 copy

Stanford University
SLAC
P. O. Box 4349
Stanford, CA 94305

Attn: W. B. Herrmannsfeldt 1 copy

Systems, Science and Software, Inc.
P. O. Box 1620
LaJolla, CA 92038

Attn: A. R. Wilson	1 copy

Texas Tech University
P. O. Box 5404 North College Station
Lubbock, TX 79417

Attn: T. L. Simpson	1 copy

TRW Defense and Space Sys Group
One Space Park
Redondo Beach, CA 90278

Attn: Tech Info Center/S-1930	1 copy
Z.G.T. Guiragossian	1 copy
D. Arnush	1 copy

University of California
Dept. of Physics
La Jolla, CA 92037

Attn: K. Brueckner	1 copy
W.B. Thompson	1 copy

University of California
Boelter Hall 7731
Los Angeles, CA 90024

Attn: F.F. Chen	1 copy

University of California
Irvine, CA 90024

Attn: G. Benford	1 copy
N. Rostoker	1 copy

University of Illinois
Urbana, IL 61801

Attn: G. H. Miley	1 copy
J. T. Verdeyen	1 copy

University of Rochester
Laboratory of Laser Energetics
River Station, Hopeman 110
Rochester, NY 14627

Attn: M. J. Lubin — 1 copy

University of Scranton
Dept. of Physics
Scranton, PA 18510

Attn: F. Murray — 1 copy

U. S. Department of Energy
P. O. Box 62
Oak Ridge, TN 37830 — 50 copies

Vought Corporation
Michigan Division
38111 Van Dyke Road
Sterling Heights, MI 48077
(Formerly LTV Aerospace Corp)

Attn: Tech Lib — 1 copy

Atomic Weapons Research Establishment
Building H36
Aldermaston, Reading RG 7 4PR
United Kingdom

Attn: J. C. Martin — 1 copy

Bhabha Atomic Research Centre
Bombay - 400085, India

Attn: B. K. Godwal — 1 copy
A. S. Paithankar — 1 copy

CEA, Centre de Etudes de Lemeil
B. P. 27
94190 Villeneuve, Saint George
France

Attn: A. Bernard — 1 copy
A. Jolas — 1 copy

CEA, Centre de Etudes de Valduc
P. B. 14
21120 Is-sur-Tille
France

Attn:	J. Barbaro	1 copy
	C. Bruno	1 copy
	N. Camarcat	1 copy
	C. Patou	1 copy
	C. Peugnet	1 copy

Centro Di Frascati
C.P.N. 65
00044 Frascati (Roma)
Italy

Attn: J.P. Rajer 1 copy

Culham Laboratories
UKAEA
Ebingdon, Birks.
England

Attn: N. J. Peacock 1 copy

Ecole Polytechnique
Labo. PMI
91128 Palaseau Cedex
France

Attn:	J. M. Buzzi	1 copy
	H. Doucet	1 copy

Ecole Polytechnique
Labo. PMI
91128 Palaseau Cedex
France

Attn:	J.M. Buzzi	1 copy
	H. Doucet	1 copy

Institut d'Electronique Fondamentale
Universite' Paris XI-Bat. 220
F91405 Orsay
France

Attn: G. Gautherin 1 copy

Institut fur Angewandte Physik
Robert Mayer Str. 2-4
D6000 Frankfurt,
West Germany

Attn:	H. Deitinghoff	1 copy
	H. Klein	1 copy

Institut Fur Neutronenphysik
un Reaktortechnik
Postfach 3640
Kernforschungszentrum
D-7500 Karisruhe 1
West Germany

Attn:	H. Bluhm	1 copy
	H. U. Karow	1 copy
	W. Schmidt	1 copy
	K.W. Zieher	1 copy

Institute of Atomic Energy
Academia Sinica
P.O. Box 2125
Beijing
People's Republic of China

Attn:	W. Ganchang, Director	2 copies
	R. Hong	1 copy

Institute of Laser Engineering
Osaka University
Yamadakami
Suita
Osaka 565, Japan

Attn:	K. Imasaki	1 copy
	S. Nakai	1 copy

Institute of Nuclear Energy Research
Atomic Energy Council
P.O. Box 3 - Lung-Tan, Taiwan
Republic of China

Attn:	C. Chang	1 copy

Instituto De Investigaciones Cientificas Y Technicas
De Las Fuerzas Armadas
Aufriategui y Varela
V. Martelli 1603
Pcia Bs. As. - R. Argentina

Attn: N. P. Camusso — 1 copy

Max-Planck-Institut fur Plasmaphysik
8046 Garching bei Munchen
West Germany

Attn: R. Lengyel — 1 copy
I. Hofmann — 1 copy

Physical Research Laboratory
Navrangpura
Ahmedabad - 380009 - India

Attn: V. Ramani — 1 copy
P. I. John — 1 copy

Shivaji University
Kolhapur, India

Attn: L. N. Katkan — 1 copy

Tokyo Institute of Technology
The Graduate School at Nagatsuta
4259 Nagatsuta, Midori-Ku
Yokohama 227, Japan

Attn: K. Niu — 1 copy
S. Yamaguchi — 1 copy

Weizmann Institute of Science
Rehovot, Israel

Attn: A. E. Blaugrund — 1 copy
E. Nardi — 1 copy
Z. Zinamon — 1 copy

Near Kanchan Bhawan
Var Ruchi Marg, Madhav Nagar,
Ujjain, (M.P.) INDIA

Attn: Dr. R. K. Chhajlani — 1 copy

JAYCOR, Inc.
11011 Torreyana Road
San Diego, CA 92121

Attn: S. S. Wang 1 copy

Los Alamos National Laboratory
P. O. Box 1663
Los Alamos, NM 87545

Attn: C. Barnes 1 copy

Mission Research Corporation
Capitol Building II, Suite 201
5503 Cherokee Avenue
Alexandria, VA 22312

Attn: B. Goplen 1 copy

Sandia National Laboratories
P. O. Box 5800
Albuquerque, NM 87185

Attn: J. Quintens/4252 1 copy

SRI International
333 Ravenswood Avenue
Menlo Park, CA 94025

Attn: R. J. Vidmar 1 copy

Stanford University
Dept. of Electrical Engineering
Stanford, CA 94305

Attn: O. Buneman 1 copy

Stanford University
Dept. of Mechanical Engineering
Stanford, CA 94305

Attn: M. Mitchner 1 copy
S. A. Self 1 copy

Stanford University
Hoover Institution
Stanford, CA 94305

Attn: D. L. Bark 1 copy

Stevens Institute of Technology
Dept of Physics
Castle Point Station
Hoboken, NJ 07030

Attn: W. Bostick 1 copy
V. Nardi 1 copy

Texas Tech University
P. O. Box 5404 - North College Station
Lubbock, TX 79417

Attn: M. Kristiansen 1 copy

US Air Force Academy
Dept. of Physics
Colorado, 80840

Attn: J. T. May 1 copy
D. Murawinski 1 copy

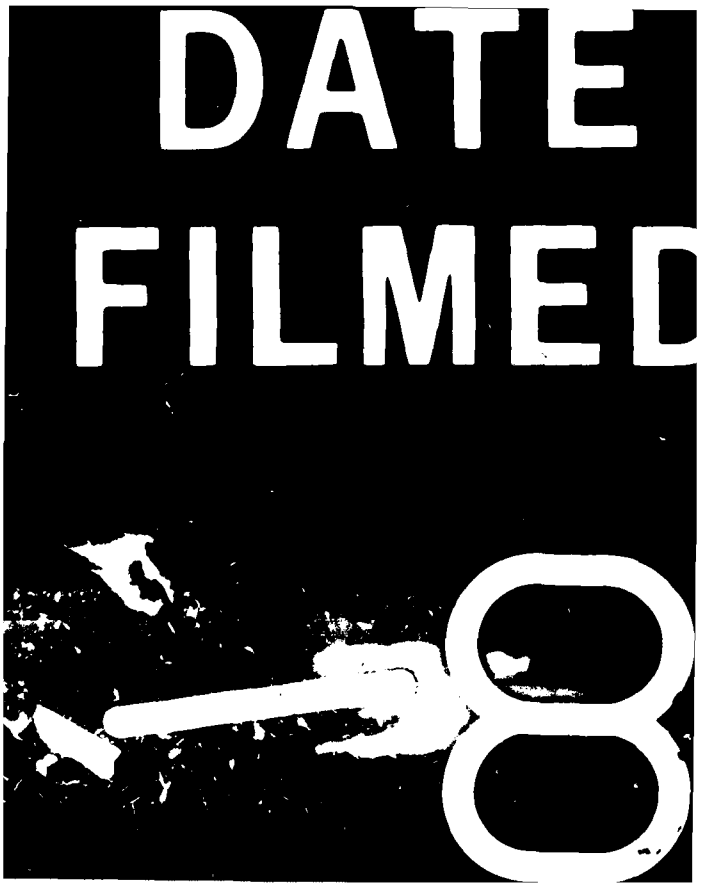
DATE
FILMED
8